On the Dependence of the Pressure on the Time Step in Incompressible Flow Simulations on Varying Spatial Meshes

Michael Besier and Winnifried Wollner

Abstract. Subject of this paper is an analysis of the behavior of the pressure on dynamically changing spatial meshes during the computation of nonstationary incompressible flows. In particular, we are concerned with discontinuous Galerkin finite element discretizations in time. Here it is observed that whenever the spatial mesh is changed between two time steps the pressure in the next time step will diverge with order k^{-1}. We will proof that this behavior is due to the fact, that discrete solenoidal fields lose this property under changes of the spatial discretization. In addition we will numerically study the fractional-step-θ scheme, and discuss why the divergence is not observed when using this time discretization. Finally we will derive a possible way to circumvent this problem.

Mathematics Subject Classification (2010). Primary 65M12, 65M60; Secondary 65M50, 76D05, 76M10.

Keywords. space-time finite elements, dynamically changing meshes, incompressible fluids, pressure approximation, backward euler, discontinuous Galerkin method in time.

1. Introduction

In this paper, we consider nonstationary incompressible flows described by the incompressible Navier-Stokes equations, given in the dimensionless form as

$$\begin{aligned} \partial_t \boldsymbol{v} - \nu \Delta \boldsymbol{v} + (\boldsymbol{v} \cdot \nabla)\boldsymbol{v} + \nabla p &= \boldsymbol{f} && \text{in } I \times \Omega, \\ \nabla \cdot \boldsymbol{v} &= 0 && \text{in } I \times \Omega, \\ \boldsymbol{v}(0) &= \boldsymbol{v^0} && \text{in } \Omega \end{aligned} \tag{1.1}$$

with a time interval $I = (0, T)$, computational domain $\Omega \subseteq \mathbb{R}^d$, $d \in \{ 2, 3 \}$, kinematic viscosity ν, volume forces $\boldsymbol{f}$, and initial values $\boldsymbol{v^0}$. These equations

have to be supplemented by appropriate boundary conditions. For sake of simplicity, we will consider no-slip Dirichlet boundary conditions.

The computational costs of numerically solving nonstationary flow problems are comparatively high due to the complex structure of such problems, especially when dealing when three-dimensional geometries. Thus, it is crucial to apply adaptive refinement techniques to reduce the size of the approximative problem without reducing the accuracy of the approximation. To be most efficient in capturing the dynamics of a nonstationary flow problem, it seems desirable to use so-called *dynamic meshes* for the discretization in space. That is, one uses possibly different meshes for different time points. Thus, one can efficiently resolve and track fronts marching through the domain, for example.

Adaptive methods are widely used in the context of finite element discretizations of partial differential equations, see, for example, [34] or [14] for an overview. Applications to nonstationary incompressible flow problems can be found, e. g., in [2], [21], or [5, 29]. However, while the usage of dynamically changing spatial meshes seems straight forward in the context of Galerkin finite element discretizations, it provides some pitfalls if one is interested in the approximation of the pressure. The aim of this paper is to describe and analyze this problem and to present a way to circumvent it. The results presented in this paper have been developed to a great extent in the PhD thesis of the first author, see [29].

The discretization of the nonstationary incompressible Navier-Stokes equations (1.1) will be done by means of space-time finite element methods. To this end, we state the variational formulation of (1.1) which reads as follows: For $\boldsymbol{f} \in L^2(I, H^{-1}(\Omega)^d)$ and $\boldsymbol{v^0} \in L^2(\Omega)^d$ find $\boldsymbol{u} \coloneqq (\boldsymbol{v}, p)^T \in X$ such that

$$\int_I \left\{ (\partial_t \boldsymbol{v}, \boldsymbol{\psi}) + \nu(\nabla \boldsymbol{v}, \nabla \boldsymbol{\psi}) + ((\boldsymbol{v} \cdot \nabla)\boldsymbol{v}, \boldsymbol{\psi}) - (p, \nabla \cdot \boldsymbol{\psi}) + (\nabla \cdot \boldsymbol{v}, \chi) \right\} \mathrm{d}t + (\boldsymbol{v}(0) - \boldsymbol{v^0}, \boldsymbol{\psi}(0)) = \int_I (\boldsymbol{f}, \boldsymbol{\psi}) \, \mathrm{d}t \quad \forall \boldsymbol{\varphi} \coloneqq (\boldsymbol{\psi}, \chi)^T \in X, \quad (1.2)$$

where $(\cdot, \cdot)$ denotes the inner product on $L^2(\Omega)$ (or $L^2(\Omega)^d$) and the space X is given as

$$X \coloneqq \Big\{ \boldsymbol{u} = (\boldsymbol{v}, p)^T \;\Big|\; \boldsymbol{v} \in L^2(I, H_0^1(\Omega)^d),\ \partial_t \boldsymbol{v} \in L^2(I, H^{-1}(\Omega)^d),\ p \in L^2(I, L^2(\Omega)/\mathbb{R}) \Big\}.$$

For questions on existence and uniqueness of solutions, we refer to [30].

Remark 1.1. In applications, we will sometimes be confronted with configurations in which Dirichlet boundary conditions for the velocity are not prescribed on the whole boundary. Instead, there will be some part Γ_{out} of the boundary representing an outlet. Then, we apply natural boundary conditions on Γ_{out}:

$$\nu \partial_{\boldsymbol{n}} \boldsymbol{v} - p\boldsymbol{n} = \boldsymbol{0}.$$

This type of boundary condition implicitly normalizes the pressure such that it is already uniquely determined without the usual mean value constraint. Hence, the spaces in which the solutions are sought have to be modified to

$$\boldsymbol{v} \in \left\{ \boldsymbol{v} \in H^1(\Omega)^d \;\middle|\; \boldsymbol{v}\big|_{\partial\Omega\setminus\Gamma_{\text{out}}} = \boldsymbol{0} \right\}, \quad p \in L^2(\Omega).$$

For more information on this free outflow boundary condition as well as results concerning existence and uniqueness of solutions, we refer to [20].

The rest of this paper is structured as follows. We start by describing the discretization of the nonstationary Navier-Stokes equations in Section 2. Then, in Section 3 we will consider a well known benchmark problem to illustrate the behavior of the pressure once the spatial discretization is changed over time. That section concludes by stating a model problem that exhibits the same behavior. We then analyze the behavior both numerically as well as analytically in Section 4. This articles concludes with Section 5 where we will demonstrate how the problem can be circumvented.

2. Discretization

In this section, we describe the discretization of the weak formulation of the time-dependent incompressible Navier-Stokes equations (1.2). The discretization in space as well as in time will be done by means of Galerkin finite element methods.

2.1. Discretization in time

For the semi-discretization in time, we use *discontinuous Galerkin* (dG) methods. To this end, we partition the time interval $\bar{I} = [0, T]$ into

$$\bar{I} = \{0\} \cup I_1 \cup \cdots \cup I_m \cup \cdots \cup I_M$$

with subintervals $I_m := (t_{m-1}, t_m]$ of length $k_m := t_m - t_{m-1}$ using time points

$$0 = t_0 < t_1 < \cdots < t_m < \cdots < t_M = T.$$

The discretization parameter k is given as a piecewise constant function by setting $k\big|_{I_m} := k_m$ for $m = 1, \ldots, M$.

The dG(r) semi-discretization of the incompressible Navier-Stokes equations (1.2) then seeks a solution $\boldsymbol{u_k} = (\boldsymbol{v_k}.p_k)^T$ which is piecewise polynomial of degree r on each subinterval I_m. For further details, we refer to [31] or [5, 29].

Remark 2.1. Due to the discontinuity of the test functions, the dG(r) discretizations decouple into time stepping schemes. For example, the dG(0) discretization is a variant of the backward Euler method, while the dG(1) discretization, after applying quadrature rules to the temporal integrals, corresponds to some implicit Runge-Kutta method.

2.2. Discretization in space

For the discretization in space of the semi-discrete problems obtained in the previous subsection, we use *continuous Galerkin* (cG) methods. To this end, we use two- or three-dimensional shape-regular meshes, see, e. g., [10]. A mesh consists of quadrilateral or hexahedral cells K which form a non-overlapping cover of the computational domain $\Omega \subseteq \mathbb{R}^d$, $d \in \{ 2, 3 \}$. The corresponding mesh is denoted by $\mathcal{T}_h = \{ K \}$, where the discretization parameter h is defined as a cellwise constant function by setting $h\big|_K = h_K$ with the diameter h_K of the cell K.

Remark 2.2. In order to ease mesh refinement, we allow cells to have nodes which lie on midpoints of faces or edges of neighboring cells. But at most one such *hanging node* is permitted on each face or edge. There are no degrees of freedom corresponding to these irregular nodes and the value of a finite element function is determined by pointwise interpolation, see [9] for more details.

On the mesh $\mathcal{T}_h$, we construct a conforming finite element space $V_h^s \subset H^1(\Omega)$ in a standard way:

$$V_h^s := \left\{ v \in C(\overline{\Omega}) \;\middle|\; v\big|_K \in \mathcal{Q}_s(K) \text{ for } K \in \mathcal{T}_h \right\} \subseteq H^1(\Omega),$$

where $\mathcal{Q}_s(K)$ denotes the space of isoparametric elements of degree s.

To obtain the formulation of the fully discrete problem, we allow dynamic mesh change in time, but the time steps k_m are kept constant in space. To this end, we associate with each time point t_m a mesh $\mathcal{T}_h^m$ and corresponding (spatial) finite element spaces $V_h^{s_{\boldsymbol{v}},m}$ and $V_h^{s_p,m}$. Finally, we set

$$H_h^m := V_h^{s_{\boldsymbol{v}},m} \cap H_0^1(\Omega) \quad \text{and} \quad L_h^m := V_h^{s_p,m} \cap L^2(\Omega)/\mathbb{R}.$$

Then, the cG(s)dG(r) discretization seeks a solution $\boldsymbol{u_{kh}} = (\boldsymbol{v_{kh}}, p_{kh})^T$ with $\boldsymbol{u_{kh}}\big|_{I_m} \in \mathcal{P}_r(I_m, (H_h^m)^d \times L_h^m)$ for each $m = 1, \ldots, M$. More details can be found again in [5, 29].

Remark 2.3. The notation cG(s)dG(r), representing a space-time finite element discretization with continuous piecewise polynomials of degree s in space and discontinuous piecewise polynomials of degree r in time, is taken from [15].

2.3. Stabilization

The fully discrete formulation does not lead to a stable approximation of problem (1.2) unless the spatial finite element spaces H_h^m and L_h^m fulfill the Babuška-Brezzi inf-sup-stability condition. This condition states (see, for example, [17]) that there is a constant β independent of h such that

$$\inf_{p_h \in L_h^m} \sup_{\boldsymbol{v_h} \in (H_h^m)^d} \frac{(p_h, \nabla \cdot \boldsymbol{v_h})}{\|p_h\| \, \|\nabla \boldsymbol{v_h}\|} \geq \beta > 0. \tag{2.1}$$

Especially the cases of equal-order trial spaces, i. e., $s_{\boldsymbol{v}} = s_p = s$, which are favorable from the implementational point of view, do not fulfill condition (2.1).

To obtain stable approximations, one has to use mixed finite element methods like the Taylor-Hood element ($s_{\boldsymbol{v}} = 2$, $s_p = 1$, for example). For more details on this topic, we refer to [22] and [7] or [17]. Alternatively one may add stabilization terms. For implementational reasons, we use equal-order trial spaces and apply the so-called *local projection stabilization* (LPS), see, e. g., [3, 4].

For the computation of the subsequent examples we used the two finite element packages deal.II [13] and Gascoigne [16].

3. Problem description and reduction to a model problem

In this section, we discuss a particular problem which arises when using dynamic meshes in the approximation of solutions of the incompressible Navier-Stokes equations. The outline of this section is as follows: In the first Subsection 3.1, we present a simulation of the benchmark problem "Laminar Flow Around a Cylinder" (see [28]) using the cG(1)dG(1) discretization on dynamic meshes. We are then concerned to consider a simpler model problem in order to analyze the effects. Hence, in Subsection 3.2, we show that the effects shown in Subsection 3.1 are not specifically related to the Navier-Stokes equations, but can already be seen when solving the linear Stokes equations on dynamic meshes. We will see that while the approximations of the velocities are quite satisfactory, the approximation of the pressure on dynamic meshes deteriorates.

3.1. Description of the problem

In this subsection, we aim at computing the lift-coefficient in the two-dimensional benchmark problem "Laminar Flow Around a Cylinder", see [28] for a detailed description of the setting as well as the precise formula for the lift-coefficient.

The time-dependent inflow condition is given by

$$v_1(t, \boldsymbol{x}) = \frac{6 \sin(\frac{\pi t}{8\,\mathrm{s}})}{(0.41\,\mathrm{m})^2} x_2 (0.41\,\mathrm{m} - x_2)\,\mathrm{m\,s^{-1}}, \quad v_2(t, \boldsymbol{x}) = 0\,\mathrm{m\,s^{-1}}$$

which yields a time-dependent Reynolds number of $0 \leq \mathrm{Re}(t) \leq 100$ for $t \in I = (0\,\mathrm{s}, 8\,\mathrm{s})$. On the outflow boundary, we apply the "do nothing" boundary condition, see [20]. On the remaining part of the boundary, no-slip boundary conditions are employed.

In this example, we apply the cG(1)dG(1) discretization. After five iterations of adaptive temporal and spatial refinement using dynamic meshes, following [5, 29], the temporal evolution of the lift-coefficient looks as depicted in Figure 1.

We note slight oscillations in the lift-coefficient, for example, near $t = 7.25\,\mathrm{s}$. Further investigations in Section 3.2 show that such oscillations especially occur when switching from one spatial mesh to another. In the following sections, we are going to numerically analyze these oscillations.

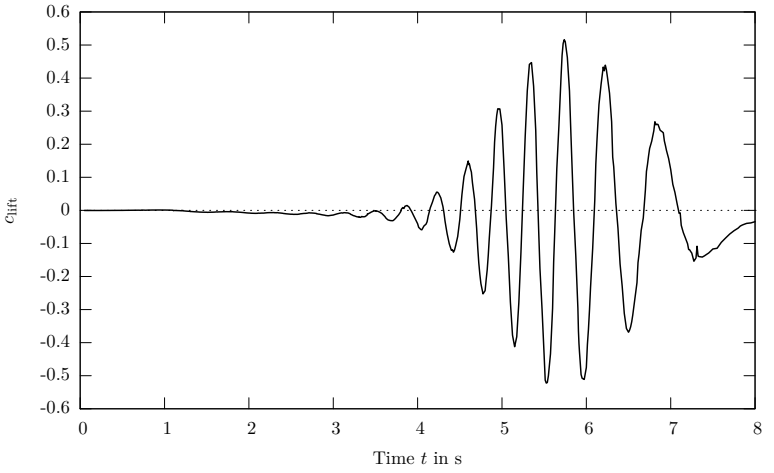

FIGURE 1. Lift-coefficient c_{lift} after five adaptation cycles

3.2. Reduction to model problem

In this section, we will show that the oscillations in the lift-coefficient shown in the last section are caused by errors located solely in the discrete pressure when switching from one spatial mesh to another. This effect can already be observed when solving the linear Stokes equations instead of the nonlinear Navier-Stokes equations. Furthermore, these errors also arise when applying uniform refinement of a mesh. We state a model problem on a polygonally bounded domain in order to avoid special effects from the approximation of a curved boundary.

Let us first show that the arising problems are not related to the time-dependent inflow boundary condition. To this end, we remove the oscillatory sine-term from the inflow condition and reduce the inflow velocity to

$$v_1(t,\boldsymbol{x}) = \frac{1.2}{(0.41\,\mathrm{m})^2}\, x_2(0.41\,\mathrm{m} - x_2)\,\mathrm{m\,s^{-1}}, \quad v_2(t,\boldsymbol{x}) = 0\,\mathrm{m\,s^{-1}}.$$

This yields a constant Reynolds number of $\mathrm{Re} = 20$ with a stationary solution. Since the effects we want to study can already be seen when working with the simplest temporal discretization, we apply the cG(1)dG(0) discretization which here coincides with the backward Euler scheme since there are no forces $\boldsymbol{f}$ depending on time. We again focus on computing the lift-coefficient whose reference value in this configuration is given as $c_{\text{lift}}^{(\text{ref})} = 0.010618948146$, see, for example [26].

We use the time interval $I = (0\,\mathrm{s}, 8\,\mathrm{s})$ with different spatial meshes. Denoting the meshes on $(2\,\mathrm{s}, 4\,\mathrm{s}] \cup (6\,\mathrm{s}, 8\,\mathrm{s}]$ with $\mathcal{T}_h$, we use the mesh $\mathcal{T}_{2h}$ on $[0\,\mathrm{s}, 2\,\mathrm{s}] \cup (4\,\mathrm{s}, 6\,\mathrm{s}]$. That is, we perform uniform refinement of the spatial mesh at $t = 2\,\mathrm{s}$ and $t = 6\,\mathrm{s}$, whereas at $t = 4\,\mathrm{s}$ uniform coarsening is applied. The evolution of the lift-coefficient for a uniform time step size of $k = 1.5625 \cdot$

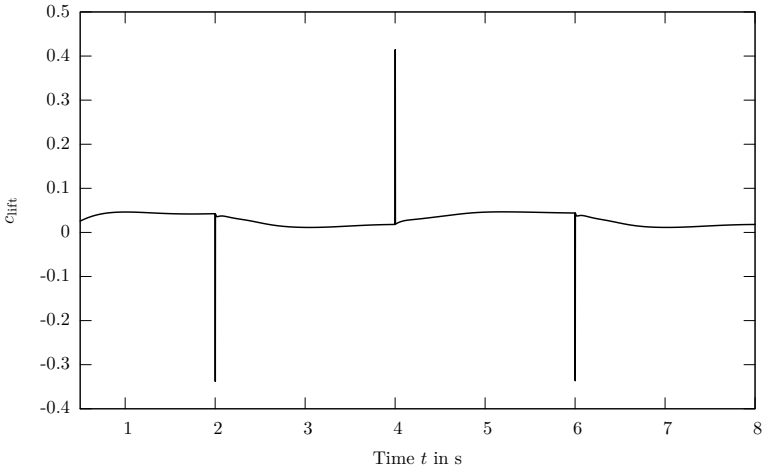

FIGURE 2. Temporal evolution of the lift-coefficient

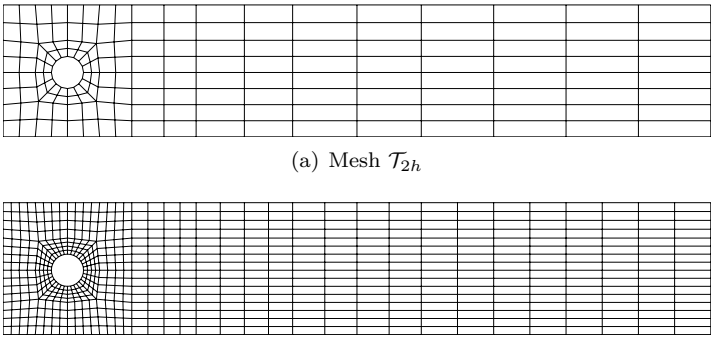

(a) Mesh $\mathcal{T}_{2h}$

(b) Mesh $\mathcal{T}_h$

FIGURE 3. Spatial meshes used for the computation of the lift-coefficient

10^{-3} s on the time interval $[0.5\,\text{s}, 8\,\text{s}]$ is shown in Figure 2. We neglect the beginning of the time interval where a singularity in the pressure evolves for $t \to 0$ due to compatibility conditions that are not fulfilled with the initial condition $\boldsymbol{v}^{\mathbf{0}} = \mathbf{0}$, see, for instance, [19]. The spatial meshes $\mathcal{T}_{2h}$ and $\mathcal{T}_h$ used in these computations are depicted in Figure 3.

We observe that precisely in the first time step on the new mesh the lift-coefficient deteriorates. We also note that these errors are even larger than in the example presented in the previous subsection.

In the remaining part of this section, we will show that these errors occurring when switching the spatial mesh are solely located in the discrete

pressure. Furthermore, we will show that these effects are not specifically related to the nonlinearity of the Navier-Stokes equations or to higher Reynolds numbers, but also arise when solving the linear Stokes equations with $\nu = 1$. Therefore, we introduce a linear model problem with known analytical (stationary) solution on a polygonally bounded domain. This simple setting allows us to study the phenomenon presented here. For sake of simplicity, we use the cG(1)dG(0) discretization here, too.

Hence, we want to find $(\boldsymbol{v}, p)^T$ such that

$$\begin{aligned} \partial_t \boldsymbol{v} - \Delta \boldsymbol{v} + \nabla p &= \boldsymbol{f} && \text{in } I \times \Omega, \\ \nabla \cdot \boldsymbol{v} &= 0 && \text{in } I \times \Omega, \\ \boldsymbol{v} &= \boldsymbol{0} && \text{in } \{\, 0 \,\} \times \Omega, \\ \boldsymbol{v} &= \boldsymbol{0} && \text{on } I \times \partial\Omega. \end{aligned} \tag{3.1}$$

Further, let $I = (0, 9)$ and $\Omega = (-1, 1)^2$. Let $\boldsymbol{f}$ be given in such a way that (3.1) possesses the stationary solution

$$\begin{aligned} \boldsymbol{v}(\boldsymbol{x}) &= \begin{pmatrix} \cos^2(\frac{\pi x_1}{2}) \cos(\frac{\pi x_2}{2}) \sin(\frac{\pi x_2}{2}) \\ -\cos(\frac{\pi x_1}{2}) \sin(\frac{\pi x_1}{2}) \cos^2(\frac{\pi x_2}{2}) \end{pmatrix}, \\ p(\boldsymbol{x}) &= \cos(\tfrac{\pi x_1}{2}) \sin(\tfrac{\pi x_1}{2}) \cos(\tfrac{\pi x_2}{2}) \sin(\tfrac{\pi x_2}{2}). \end{aligned}$$

We subdivide $\bar{I} = I^{(1)} \cup I^{(2)} \cup I^{(3)}$ with

$$I^{(1)} = [0, 3], \quad I^{(2)} = (3, 6], \quad I^{(3)} = (6, 9].$$

On $I^{(1)}$ and $I^{(3)}$ we use a uniform spatial mesh of cell size $2h$, whereas on the subinterval $I^{(2)}$ a uniform spatial mesh of cell size h is used. That is, we switch the spatial mesh uniformly from $2h$ to h at $t = 3$ and from h to $2h$ at $t = 6$. The subintervals are chosen long enough for the discrete solution to reach the stationary limit on each mesh.

The errors $\left\|\nabla(\boldsymbol{v} - \boldsymbol{v_{kh}})\right\|$ and $\|p - p_{kh}\|$ for a uniform step size of $k \approx 2 \cdot 10^{-4}$ and mesh size $h = 2^{-4}$ are shown in Figure 4. As we can see, both the velocity and the pressure approximation show a transient phenomenon when switching the spatial mesh. However, while the approximation of the velocity component is quite satisfactory, the transient phenomenon in the pressure component is superposed by an additional error which causes the approximation of the pressure to deteriorate under a change of the spatial mesh, see Figure 5. The larger errors near $t = 0$ stem from the fact that we do not start the simulation with the stationary solution, but rather with $\boldsymbol{v^0} = \boldsymbol{0}$. Hence the error compared to the stationary limit is large.

In the next section, we will further analyze how these errors behave under systematic refinement of the temporal and spatial discretization.

4. Analysis of the problem

Subsection 4.1 focuses on the precise numerical analysis of the error that occurs after changing the spatial mesh. To this end, we apply the cG(s)dG(0)

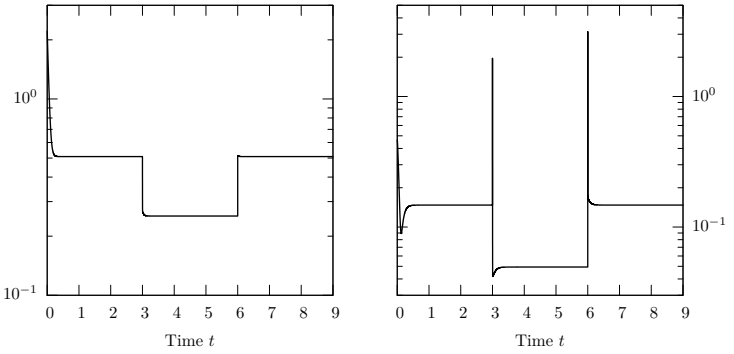

FIGURE 4. Errors $\left\|\nabla(\boldsymbol{v} - \boldsymbol{v_{kh}})\right\|$ (left) and $\|p - p_{kh}\|$ (right)

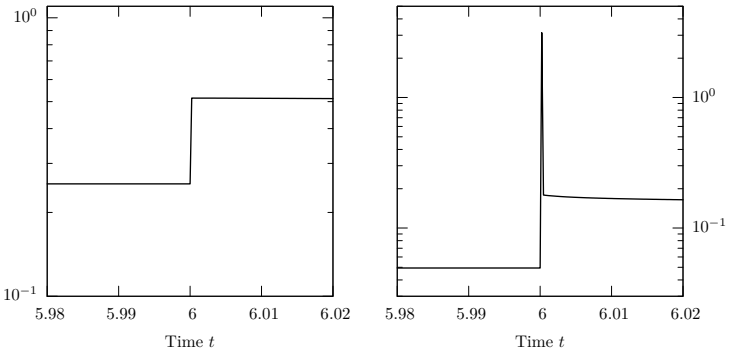

FIGURE 5. Errors $\left\|\nabla(\boldsymbol{v} - \boldsymbol{v_{kh}})\right\|$ (left) and $\|p - p_{kh}\|$ (right) near $t = 6$

and the cG(s)dG(1) discretization to our model problem. We especially investigate the behavior of the error under systematic refinement of the temporal and the spatial discretization. Furthermore, we present some results using the inf-sup-stable $\mathcal{Q}_2/\mathcal{Q}_1$-Taylor-Hood element (see, for instance, [22]) for the spatial discretization to show that the effects are not induced by stabilization. Finally in Subsection 4.2, we analytically investigate the phenomenon discussed in this article.

4.1. Behavior of the error under temporal and spatial refinement

In this subsection, we numerically analyze the behavior of the error described in the last section. We especially consider systematic uniform refinement of the temporal and spatial discretization. The analysis will be done by means of the model problem presented in the previous section. Thereby, we are going to consider the equal-order cG(1) and cG(2) discretizations in space together with the local projection stabilization as well as the inf-sup-stable $\mathcal{Q}_2/\mathcal{Q}_1$-Taylor-Hood element. For the temporal discretization we will apply

TABLE 1. $\|p - p_{kh}\|$ under spatial refinement for the dG(0) time discretization with different spatial discretizations

level	cG(1)		cG(2)		$\mathcal{Q}_2/\mathcal{Q}_1$	
	$t = 3 + k$	$t = 6 + k$	$t = 3 + k$	$t = 6 + k$	$t = 3 + k$	$t = 6 + k$
1	$2.88 \cdot 10^{-1}$	$4.94 \cdot 10^{-1}$	$2.44 \cdot 10^{-2}$	$5.47 \cdot 10^{-2}$	$2.95 \cdot 10^{-2}$	$5.19 \cdot 10^{-2}$
2	$5.67 \cdot 10^{-2}$	$1.82 \cdot 10^{-1}$	$3.41 \cdot 10^{-3}$	$1.21 \cdot 10^{-2}$	$2.81 \cdot 10^{-3}$	$9.15 \cdot 10^{-3}$
3	$1.89 \cdot 10^{-2}$	$5.74 \cdot 10^{-2}$	$7.45 \cdot 10^{-4}$	$2.95 \cdot 10^{-3}$	$5.24 \cdot 10^{-4}$	$2.08 \cdot 10^{-3}$
4	$6.00 \cdot 10^{-3}$	$1.77 \cdot 10^{-2}$	$1.84 \cdot 10^{-4}$	$7.36 \cdot 10^{-4}$	$1.27 \cdot 10^{-4}$	$5.10 \cdot 10^{-4}$
order	1.66	1.70	2.02	2.00	2.04	2.03

the dG(0) and dG(1) method as well as the fractional-step-θ scheme, which is a popular time-stepping scheme often used in computational fluid dynamics, see [8], [18], [25] or [32, 33].

In what follows, the behavior of the error in the pressure under systematic uniform refinement of the spatial or the temporal discretization is studied for different spatial and temporal discretizations. Since the error is concentrated to the first time step on a new mesh, we especially focus on its development there.

4.1.1. Spatial refinement. This subsection is dedicated to the numerical analysis of the error in the pressure under uniform refinement of the spatial discretization. To this end, we fix the temporal discretization which is either the dG(0), dG(1), or fractional-step-θ method. We always use a uniform time step size of $k = 3 \cdot 10^{-2}$. As in the previous section, we use the mesh $\mathcal{T}_{2h}$ on $I^{(1)}$ and $I^{(3)}$, whereas on $I^{(2)}$ the mesh $\mathcal{T}_h$ is used. We study the development of the error in the pressure component for $h \to 0$.

When using the dG(0) discretization in time, we obtain the results shown in Table 1. The corresponding results for the dG(1) time discretization are given in Table 2. Using the fractional-step-θ scheme for the temporal discretization leads to the results which are presented in Table 3. Since the mesh size of the initial coarse grid is $h = \frac{1}{4}$, refinement level 1 corresponds to $h = \frac{1}{8}$ and $2h = \frac{1}{4}$, refinement level 2 corresponds to $h = \frac{1}{16}$ and $2h = \frac{1}{8}$, etc. The orders of convergence given in the last lines are numerically computed from the values on the two finest discretizations.

We can conclude that the error in the pressure component in the first time step on a new spatial mesh converges for $h \to 0$ (at least) with the same order as the overall spatial discretization error.

4.1.2. Temporal refinement. In this subsection, the development of the pressure error under systematic uniform refinement of the temporal discretization is considered, that is we consider the case $k \to 0$. To this end, we fix the spatial discretization which is either the equal-order cG(1) or cG(2) method together with local projection stabilization or the inf-sup-stable $\mathcal{Q}_2/\mathcal{Q}_1$-Taylor-Hood element. The spatial mesh $\mathcal{T}_h$ used on the subintervals $I^{(2)}$ is given by two

TABLE 2. $\|p - p_{kh}\|$ under spatial refinement for the dG(1) time discretization with different spatial discretizations

level	cG(1)		cG(2)		$\mathcal{Q}_2/\mathcal{Q}_1$	
	$t = 3 + k$	$t = 6 + k$	$t = 3 + k$	$t = 6 + k$	$t = 3 + k$	$t = 6 + k$
1	$4.51 \cdot 10^{-1}$	$4.78 \cdot 10^{-1}$	$4.34 \cdot 10^{-2}$	$4.53 \cdot 10^{-2}$	$5.41 \cdot 10^{-2}$	$3.85 \cdot 10^{-2}$
2	$3.96 \cdot 10^{-2}$	$1.31 \cdot 10^{-1}$	$4.53 \cdot 10^{-3}$	$1.19 \cdot 10^{-2}$	$4.28 \cdot 10^{-3}$	$8.74 \cdot 10^{-3}$
3	$1.51 \cdot 10^{-2}$	$4.87 \cdot 10^{-2}$	$7.75 \cdot 10^{-4}$	$2.95 \cdot 10^{-3}$	$5.68 \cdot 10^{-4}$	$2.07 \cdot 10^{-3}$
4	$5.81 \cdot 10^{-3}$	$1.73 \cdot 10^{-2}$	$1.85 \cdot 10^{-4}$	$7.36 \cdot 10^{-4}$	$1.28 \cdot 10^{-4}$	$5.10 \cdot 10^{-4}$
order	1.38	1.49	2.07	2.00	2.15	2.02

TABLE 3. $\|p - p_{kh}\|$ under spatial refinement for the fractional-step-θ time discretization with different spatial discretizations

level	cG(1)		cG(2)		$\mathcal{Q}_2/\mathcal{Q}_1$	
	$t = 3 + k$	$t = 6 + k$	$t = 3 + k$	$t = 6 + k$	$t = 3 + k$	$t = 6 + k$
1	$8.00 \cdot 10^{-2}$	$3.45 \cdot 10^{-1}$	$1.04 \cdot 10^{-2}$	$4.43 \cdot 10^{-2}$	$9.27 \cdot 10^{-3}$	$4.46 \cdot 10^{-2}$
2	$3.27 \cdot 10^{-2}$	$1.40 \cdot 10^{-1}$	$2.51 \cdot 10^{-3}$	$9.76 \cdot 10^{-3}$	$2.11 \cdot 10^{-3}$	$8.72 \cdot 10^{-3}$
3	$1.34 \cdot 10^{-2}$	$4.24 \cdot 10^{-2}$	$6.25 \cdot 10^{-4}$	$2.39 \cdot 10^{-3}$	$5.33 \cdot 10^{-4}$	$2.07 \cdot 10^{-3}$
4	$5.15 \cdot 10^{-3}$	$1.40 \cdot 10^{-2}$	$1.50 \cdot 10^{-4}$	$5.96 \cdot 10^{-4}$	$1.28 \cdot 10^{-4}$	$5.10 \cdot 10^{-4}$
order	1.38	1.60	2.06	2.00	2.06	2.02

TABLE 4. $\|p - p_{kh}\|$ under temporal refinement for the cG(1) discretization with different temporal discretizations

level	dG(0)		dG(1)		fractional-step-θ	
	$t = 3 + k$	$t = 6 + k$	$t = 3 + k$	$t = 6 + k$	$t = 3 + k$	$t = 6 + k$
1	$3.12 \cdot 10^{-1}$	$5.16 \cdot 10^{-1}$	$4.75 \cdot 10^{-1}$	$6.39 \cdot 10^{-1}$	$1.04 \cdot 10^{-1}$	$1.48 \cdot 10^{-1}$
2	$5.52 \cdot 10^{-1}$	$8.86 \cdot 10^{-1}$	$9.83 \cdot 10^{-1}$	$1.39 \cdot 10^{+0}$	$1.75 \cdot 10^{-1}$	$1.49 \cdot 10^{-1}$
3	$1.02 \cdot 10^{+0}$	$1.63 \cdot 10^{+0}$	$1.97 \cdot 10^{+0}$	$2.89 \cdot 10^{+0}$	$2.33 \cdot 10^{-1}$	$1.49 \cdot 10^{-1}$
4	$1.96 \cdot 10^{+0}$	$3.14 \cdot 10^{+0}$	$3.90 \cdot 10^{+0}$	$5.90 \cdot 10^{+0}$	$2.71 \cdot 10^{-1}$	$1.49 \cdot 10^{-1}$
order	−0.94	−0.95	−0.99	−1.03	−0.22	0.00

uniform refinements of the coarse grid, i. e., $h = \frac{1}{16}$. On the subintervals $I^{(1)}$ and $I^{(3)}$ the corresponding mesh $\mathcal{T}_{2h}$ is employed.

For the cG(1) discretization in space, we obtain the results of Table 4. The corresponding results for the cG(2) discretization are given in Table 5, whereas Table 6 shows the results obtained with the inf-sup-stable $\mathcal{Q}_2/\mathcal{Q}_1$-Taylor-Hood element. Here, refinement level 1 corresponds to a time step size of $k = 1.875 \cdot 10^{-3}$, refinement level 2 to $k = 9.375 \cdot 10^{-4}$, etc. As in the previous subsection, the order of convergence is numerically computed from the values of the two finest discretizations.

TABLE 5. $\|p - p_{kh}\|$ under temporal refinement for the cG(2) discretization with different temporal discretizations

level	dG(0)		dG(1)		fractional-step-θ	
	$t = 3 + k$	$t = 6 + k$	$t = 3 + k$	$t = 6 + k$	$t = 3 + k$	$t = 6 + k$
1	$2.56 \cdot 10^{-2}$	$2.38 \cdot 10^{-2}$	$4.31 \cdot 10^{-2}$	$3.15 \cdot 10^{-2}$	$5.41 \cdot 10^{-3}$	$1.07 \cdot 10^{-2}$
2	$4.87 \cdot 10^{-2}$	$4.00 \cdot 10^{-2}$	$8.66 \cdot 10^{-2}$	$6.12 \cdot 10^{-2}$	$8.44 \cdot 10^{-3}$	$1.16 \cdot 10^{-2}$
3	$9.38 \cdot 10^{-2}$	$7.28 \cdot 10^{-2}$	$1.75 \cdot 10^{-1}$	$1.24 \cdot 10^{-1}$	$1.05 \cdot 10^{-2}$	$1.24 \cdot 10^{-2}$
4	$1.83 \cdot 10^{-1}$	$1.38 \cdot 10^{-1}$	$3.54 \cdot 10^{-1}$	$2.54 \cdot 10^{-1}$	$1.16 \cdot 10^{-2}$	$1.29 \cdot 10^{-2}$
order	-0.96	-0.92	-1.02	-1.03	-0.14	-0.06

TABLE 6. $\|p - p_{kh}\|$ under temporal refinement for the $\mathcal{Q}_2/\mathcal{Q}_1$ discretization with different temporal discretizations

level	dG(0)		dG(1)		fractional-step-θ	
	$t = 3 + k$	$t = 6 + k$	$t = 3 + k$	$t = 6 + k$	$t = 3 + k$	$t = 6 + k$
1	$2.80 \cdot 10^{-2}$	$2.35 \cdot 10^{-2}$	$4.70 \cdot 10^{-2}$	$2.97 \cdot 10^{-2}$	$5.26 \cdot 10^{-3}$	$1.00 \cdot 10^{-2}$
2	$5.35 \cdot 10^{-2}$	$4.05 \cdot 10^{-2}$	$9.42 \cdot 10^{-2}$	$5.94 \cdot 10^{-2}$	$8.33 \cdot 10^{-3}$	$1.12 \cdot 10^{-2}$
3	$1.03 \cdot 10^{-1}$	$7.38 \cdot 10^{-2}$	$1.91 \cdot 10^{-1}$	$1.23 \cdot 10^{-1}$	$1.04 \cdot 10^{-2}$	$1.22 \cdot 10^{-2}$
4	$2.01 \cdot 10^{-1}$	$1.40 \cdot 10^{-1}$	$3.85 \cdot 10^{-1}$	$2.51 \cdot 10^{-1}$	$1.15 \cdot 10^{-2}$	$1.28 \cdot 10^{-2}$
order	-0.96	-0.92	-1.01	-1.03	-0.15	-0.07

We observe that under uniform refinement of the temporal discretization the error in the pressure component when uniformly refining the spatial mesh increases like $O(k^{-1})$ for the dG(0) and the dG(1) discretization whereas for the fractional-step-θ scheme this error is almost independent of k. The reason for this behavior of the fractional-step-θ scheme will be clarified in Remark 5.1. For uniform coarsening of the spatial mesh we observe the same behavior.

Since the support of this error is exactly one time step, this shows the behavior of a Dirac approximation and hence the error, for example, in mean functional values involving the pressure, does not vanish for $k \to 0$.

4.2. Theoretical investigation

This section presents a theoretical investigation of the behavior of the pressure approximation when switching the spatial mesh. To this end, we consider the inf-sup-stable $\mathcal{Q}_2/\mathcal{Q}_1$-Taylor-Hood element for the spatial discretization in combination with the backward Euler time-stepping scheme. As our numerical results indicate it will be sufficient to consider one step of the backward Euler method during which the spatial discretization is changed to explain the undesired behavior of the pressure. As in the previous subsections, we consider uniform refinement or coarsening of a uniformly refined mesh. Furthermore, we assume the domain $\Omega \subseteq \mathbb{R}^d$, $d \in \{ 2, 3 \}$, to be polygonally bounded and convex.

Let $(\boldsymbol{v}, p)^T \in H_0^1(\Omega)^d \times L^2(\Omega)/\mathbb{R}$ be the unique solution of the stationary Stokes problem for $\nu = 1$:

$$\begin{aligned} (\nabla \boldsymbol{v}, \nabla \boldsymbol{\psi}) - (p, \nabla \cdot \boldsymbol{\psi}) &= (\boldsymbol{f}, \boldsymbol{\psi}) \qquad && \forall \boldsymbol{\psi} \in H_0^1(\Omega)^d, \\ (\nabla \cdot \boldsymbol{v}, \chi) &= 0 && \forall \chi \in L^2(\Omega)/\mathbb{R}. \end{aligned} \tag{4.1}$$

Then, this solution also satisfies $(\boldsymbol{v}, p)^T \in H^2(\Omega)^d \times H^1(\Omega)$ as well as the a priori estimate

$$\|\boldsymbol{v}\|_{H^2(\Omega)} + \|p\|_{H^1} \leq C \|\boldsymbol{f}\|, \tag{4.2}$$

see [24] and [12].

Let a uniform decomposition $\mathcal{T}_H$ of $\Omega \subseteq \mathbb{R}^d$ into cells be given. We define the following conforming finite element spaces for the Taylor-Hood element:

$$\begin{aligned} H_H &\coloneqq \left\{ v_H \in C(\overline{\Omega}) \;\middle|\; v_H\big|_K \in \mathcal{Q}_2(K) \; \forall K \in \mathcal{T}_H \right\} \cap H_0^1(\Omega), \\ L_H &\coloneqq \left\{ p_H \in C(\overline{\Omega}) \;\middle|\; p_H\big|_K \in \mathcal{Q}_1(K) \; \forall K \in \mathcal{T}_H \right\} \cap L^2(\Omega)/\mathbb{R}. \end{aligned}$$

Let $(\boldsymbol{v_H}, p_H)^T \in H_H^d \times L_H$ be the approximate solution on the mesh $\mathcal{T}_H$, that is

$$\begin{aligned} (\nabla \boldsymbol{v_H}, \nabla \boldsymbol{\psi}) - (p_H, \nabla \cdot \boldsymbol{\psi}) &= (\boldsymbol{f}, \boldsymbol{\psi}) \qquad && \forall \boldsymbol{\psi} \in H_H^d, \\ (\nabla \cdot \boldsymbol{v_H}, \chi) &= 0 && \forall \chi \in L_H. \end{aligned} \tag{4.3}$$

Uniformly refining or coarsening the mesh $\mathcal{T}_H$ yields a spatial mesh $\mathcal{T}_h$ and the corresponding finite element spaces

$$\begin{aligned} H_h &\coloneqq \left\{ v_h \in C(\overline{\Omega}) \;\middle|\; v_h\big|_K \in \mathcal{Q}_2(K) \; \forall K \in \mathcal{T}_h \right\} \cap H_0^1(\Omega), \\ L_h &\coloneqq \left\{ p_h \in C(\overline{\Omega}) \;\middle|\; p_h\big|_K \in \mathcal{Q}_1(K) \; \forall K \in \mathcal{T}_h \right\} \cap L^2(\Omega)/\mathbb{R}. \end{aligned}$$

Performing one backward Euler step with step size k, seeks the solution $(\boldsymbol{v_h^k}, p_h^k)^T \in H_h^d \times L_h$ of

$$\begin{aligned} \frac{1}{k}(\boldsymbol{v_h^k}, \boldsymbol{\psi}) + (\nabla \boldsymbol{v_h^k}, \nabla \boldsymbol{\psi}) & \\ - (p_h^k, \nabla \cdot \boldsymbol{\psi}) = \frac{1}{k}(\boldsymbol{v_H}, \boldsymbol{\psi}) + (\boldsymbol{f}, \boldsymbol{\psi}) \qquad && \forall \boldsymbol{\psi} \in H_h^d, \\ (\nabla \cdot \boldsymbol{v_h^k}, \chi) = 0 && \forall \chi \in L_h. \end{aligned} \tag{4.4}$$

Using the H-projection $\widetilde{\boldsymbol{P}}_{\boldsymbol{h}} \boldsymbol{v_H}$ of $\boldsymbol{v_H}$ into H_h^d as initial value in the backward Euler step, yields the solution $(\hat{\boldsymbol{v}}_{\boldsymbol{h}}^{\boldsymbol{k}}, \hat{p}_h^k)^T \in H_h^d \times L_h$ of

$$\begin{aligned} \frac{1}{k}(\hat{\boldsymbol{v}}_{\boldsymbol{h}}^{\boldsymbol{k}}, \boldsymbol{\psi}) + (\nabla \hat{\boldsymbol{v}}_{\boldsymbol{h}}^{\boldsymbol{k}}, \nabla \boldsymbol{\psi}) & \\ - (\hat{p}_h^k, \nabla \cdot \boldsymbol{\psi}) = \frac{1}{k}(\widetilde{\boldsymbol{P}}_{\boldsymbol{h}} \boldsymbol{v_H}, \boldsymbol{\psi}) + (\boldsymbol{f}, \boldsymbol{\psi}) \qquad && \forall \boldsymbol{\psi} \in H_h^d, \\ (\nabla \cdot \hat{\boldsymbol{v}}_{\boldsymbol{h}}^{\boldsymbol{k}}, \chi) = 0 && \forall \chi \in L_h. \end{aligned} \tag{4.5}$$

Here, $\widetilde{\boldsymbol{P}}_{\boldsymbol{h}}\boldsymbol{v}_{\boldsymbol{H}}$ is given as the first component of the solution $(\widetilde{\boldsymbol{P}}_{\boldsymbol{h}}\boldsymbol{v}_{\boldsymbol{H}}, \tilde{p}_h^H)^T \in H_h^d \times L_h$ of

$$\begin{aligned} (\widetilde{\boldsymbol{P}}_{\boldsymbol{h}}\boldsymbol{v}_{\boldsymbol{H}}, \boldsymbol{\psi}) - (\tilde{p}_h^H, \nabla \cdot \boldsymbol{\psi}) &= (\boldsymbol{v}_{\boldsymbol{H}}, \boldsymbol{\psi}) \qquad \forall \boldsymbol{\psi} \in H_h^d, \\ (\nabla \cdot \widetilde{\boldsymbol{P}}_{\boldsymbol{h}}\boldsymbol{v}_{\boldsymbol{H}}, \chi) &= 0 \qquad \forall \chi \in L_h. \end{aligned} \tag{4.6}$$

Lemma 4.1. *The functions $\boldsymbol{v}_{\boldsymbol{h}}^{\boldsymbol{k}}$ defined by (4.4) and $\hat{\boldsymbol{v}}_{\boldsymbol{h}}^{\boldsymbol{k}}$ defined by (4.5) coincide. Further, there exists a function $\boldsymbol{v}_{\boldsymbol{h}}^{\boldsymbol{0}} \in H_h^d$ and a sequence $k \to 0$ such that the sequence $\boldsymbol{v}_{\boldsymbol{h}}^{\boldsymbol{k}}$ fulfills*

$$\left\| \boldsymbol{v}_{\boldsymbol{h}}^{\boldsymbol{k}} - \boldsymbol{v}_{\boldsymbol{h}}^{\boldsymbol{0}} \right\| \to 0 \quad (k \to 0).$$

Proof. If we subtract equation (4.5) from (4.4), we obtain

$$\begin{aligned} \frac{1}{k}(\boldsymbol{v}_{\boldsymbol{h}}^{\boldsymbol{k}} - \hat{\boldsymbol{v}}_{\boldsymbol{h}}^{\boldsymbol{k}}, \boldsymbol{\psi}) + (\nabla(\boldsymbol{v}_{\boldsymbol{h}}^{\boldsymbol{k}} - \hat{\boldsymbol{v}}_{\boldsymbol{h}}^{\boldsymbol{k}}), \nabla\boldsymbol{\psi}) & \\ - (p_h^k - \hat{p}_h^k, \nabla \cdot \boldsymbol{\psi}) = -\frac{1}{k}(\tilde{p}_h^H, \nabla \cdot \boldsymbol{\psi}) \ \forall \boldsymbol{\psi} \in H_h^d, & \\ (\nabla \cdot (\boldsymbol{v}_{\boldsymbol{h}}^{\boldsymbol{k}} - \hat{\boldsymbol{v}}_{\boldsymbol{h}}^{\boldsymbol{k}}), \chi) = 0 \qquad \forall \chi \in L_h, & \end{aligned} \tag{4.7}$$

where we have applied (4.6) to obtain the right-hand side. Testing (4.7) with $\boldsymbol{\psi} = \boldsymbol{v}_{\boldsymbol{h}}^{\boldsymbol{k}} - \hat{\boldsymbol{v}}_{\boldsymbol{h}}^{\boldsymbol{k}} \in H_h^d$ and $\chi = p_h^k - \hat{p}_h^k$ leads to

$$\frac{1}{k}\left\| \boldsymbol{v}_{\boldsymbol{h}}^{\boldsymbol{k}} - \hat{\boldsymbol{v}}_{\boldsymbol{h}}^{\boldsymbol{k}} \right\|^2 + \left\| \nabla(\boldsymbol{v}_{\boldsymbol{h}}^{\boldsymbol{k}} - \hat{\boldsymbol{v}}_{\boldsymbol{h}}^{\boldsymbol{k}}) \right\|^2 = 0,$$

where the other terms cancel out due to the second equation of (4.7). Hence, we have $\boldsymbol{v}_{\boldsymbol{h}}^{\boldsymbol{k}} = \hat{\boldsymbol{v}}_{\boldsymbol{h}}^{\boldsymbol{k}}$.

When testing equation (4.4) with $\boldsymbol{\psi} = \boldsymbol{v}_{\boldsymbol{h}}^{\boldsymbol{k}}$ and $\chi = p_h^k$, we obtain

$$\frac{1}{k}\left\| \boldsymbol{v}_{\boldsymbol{h}}^{\boldsymbol{k}} \right\|^2 + \left\| \nabla \boldsymbol{v}_{\boldsymbol{h}}^{\boldsymbol{k}} \right\|^2 = \frac{1}{k}(\boldsymbol{v}_{\boldsymbol{H}}, \boldsymbol{v}_{\boldsymbol{h}}^{\boldsymbol{k}}) + (\boldsymbol{f}, \boldsymbol{v}_{\boldsymbol{h}}^{\boldsymbol{k}})$$

and hence

$$\left\| \boldsymbol{v}_{\boldsymbol{h}}^{\boldsymbol{k}} \right\| \leq \|\boldsymbol{v}_{\boldsymbol{H}}\| + k \|\boldsymbol{f}\|.$$

Since $\boldsymbol{v}_{\boldsymbol{H}}$ and $\boldsymbol{f}$ do not depend on time, we conclude that $\left\| \boldsymbol{v}_{\boldsymbol{h}}^{\boldsymbol{k}} \right\|$ remains bounded for $k \to 0$. Hence, there is at least one sequence $k \to 0$ and a function $\boldsymbol{v}_{\boldsymbol{h}}^{\boldsymbol{0}} \in H_h^d$ such that

$$\left\| \boldsymbol{v}_{\boldsymbol{h}}^{\boldsymbol{k}} - \boldsymbol{v}_{\boldsymbol{h}}^{\boldsymbol{0}} \right\| \to 0 \quad (k \to 0).$$

□

Since H_h^d is finite dimensional, $\boldsymbol{v}_{\boldsymbol{h}}^{\boldsymbol{k}}$ converges to $\boldsymbol{v}_{\boldsymbol{h}}^{\boldsymbol{0}}$ in every norm, even point-wise. For the following we define the L^2-projection $\boldsymbol{P}_{\boldsymbol{h}} \colon L^2(\Omega)^d \to H_h^d$ as usual by

$$(\boldsymbol{P}_{\boldsymbol{h}}\boldsymbol{f}, \boldsymbol{\psi}) = (\boldsymbol{f}, \boldsymbol{\psi}) \quad \forall \boldsymbol{\psi} \in H_h^d.$$

We are now prepared to proof the observed divergence of the pressure as $k \to 0$.

Lemma 4.2. *The function* $\boldsymbol{v_h^0} \in H_h^d$ *given by Lemma* 4.1 *is uniquely determined by* $\boldsymbol{v_h^0} = \widetilde{\boldsymbol{P}}_{\boldsymbol{h}} \boldsymbol{v_H}$. *Let* $p_h^k \in L_h$ *be given by* (4.4), *then either*

$$a)\ \widetilde{\boldsymbol{P}}_{\boldsymbol{h}} \boldsymbol{v_H} = \boldsymbol{P_h v_H} \quad or \quad b)\ \left\| p_h^k \right\| \geq C \frac{1}{k}$$

with some constant $C > 0$ *independent of* k.

Proof. Let $\boldsymbol{v_h^0} \in H_h^d$ and $k \to 0$ be any sequence such that $\boldsymbol{v_h^k} \to \boldsymbol{v_h^0}$, the existence of such objects is ensured by Lemma 4.1.

We note that (4.4) is equivalent to the algebraic system

$$\begin{pmatrix} \boldsymbol{M} + k\boldsymbol{A} & k\boldsymbol{B} \\ -\boldsymbol{B}^T & 0 \end{pmatrix} \begin{pmatrix} \boldsymbol{x^k} \\ \boldsymbol{y^k} \end{pmatrix} = \begin{pmatrix} \boldsymbol{b^k} \\ 0 \end{pmatrix} \tag{4.8}$$

with

$$\boldsymbol{M} = \big((\boldsymbol{\psi_j}, \boldsymbol{\psi_i})\big)_{i,j=1,\dots,N_H}, \quad \boldsymbol{A} = \big((\nabla \boldsymbol{\psi_j}, \nabla \boldsymbol{\psi_i})\big)_{i,j=1,\dots,N_H},$$
$$\boldsymbol{B} = \big(-(\chi_j, \nabla \cdot \boldsymbol{\psi_i})\big)_{\substack{i=1,\dots,N_H, \\ j=1,\dots,N_L}}$$

and right-hand side

$$\boldsymbol{b^k} = \big((\boldsymbol{v_H}, \boldsymbol{\psi_i}) + k(\boldsymbol{f}, \boldsymbol{\psi_i})\big)_{i=1,\dots,N_H}$$

where we use the representations

$$\boldsymbol{v_h^k} = \sum_{j=1}^{N_H} x_j^k \boldsymbol{\psi_j} \quad \text{and} \quad p_h^k = \sum_{j=1}^{N_L} y_j^k \chi_j.$$

Here, $\left\{ \boldsymbol{\psi_j} \;\middle|\; j = 1, \dots, N_H \right\}$ is a basis of H_h^d while $\left\{ \chi_j \;\middle|\; j = 1, \dots, N_L \right\}$ is a basis of L_h. This especially means

$$\boldsymbol{M x^k} + k\boldsymbol{A x^k} + k\boldsymbol{B y^k} = \boldsymbol{b^k}. \tag{4.9}$$

Since $\boldsymbol{v_h^k}$ converges point-wise to $\boldsymbol{v_h^0}$, we have $\boldsymbol{x^k} \to \boldsymbol{x^0}$ with

$$\boldsymbol{v_h^0} = \sum_{j=1}^{N_H} x_j^0 \boldsymbol{\psi_j}.$$

For $k \to 0$, we have

$$\boldsymbol{b^k} \to \boldsymbol{b^0} = \big((\boldsymbol{v_H}, \boldsymbol{\psi_i})\big)_{i=1,\dots,N_H} = \boldsymbol{M}\bar{\boldsymbol{x}},$$

because $\boldsymbol{v_H}$ and $\boldsymbol{f}$ do not depend on time, and $\bar{\boldsymbol{x}} \in \mathbb{R}^{N_H}$ is given by

$$\boldsymbol{P_h v_H} = \sum_{j=1}^{N_H} \bar{x}_j \boldsymbol{\psi_j}.$$

In virtue of (4.9), we conclude that $k\boldsymbol{y^k}$ converges for $k \to 0$, too. By passing to the limit $k \to 0$ in (4.9), we obtain

$$\boldsymbol{M x^0} + \boldsymbol{B y^0} = \boldsymbol{M}\bar{\boldsymbol{x}}. \tag{4.10}$$

where $\boldsymbol{y^0}$ is the limit of $k\boldsymbol{y^k}$ for $k \to 0$. Equation (4.10) may equivalently be written as

$$(\boldsymbol{v_h^0}, \boldsymbol{\psi}) - (p_h^0, \nabla \cdot \boldsymbol{\psi}) = (\boldsymbol{P_h v_H}, \boldsymbol{\psi}) = (\boldsymbol{v_H}, \boldsymbol{\psi}) \quad \forall \boldsymbol{\psi} \in H_h^d,$$

which together with the second equation in (4.8) states that $\boldsymbol{v_h^0}$ is just the H-projection of $\boldsymbol{v_H}$ into H_h^d. In particular $\boldsymbol{v_h^0}$ is uniquely determined and convergence in Lemma 4.1 is obtained for any sequence $k \to 0$.

The Lagrange multiplier $p_h^0 \in L_h$ herein is given as

$$p_h^0 = \sum_{j=1}^{N_L} y_j^0 \chi_j.$$

To continue we note that if $\boldsymbol{y^0} = \boldsymbol{0}$, we then have $\boldsymbol{x^0} = \bar{\boldsymbol{x}}$ or equivalently $\boldsymbol{P_h v_H} = \boldsymbol{v_h^0} = \widetilde{\boldsymbol{P}}_{\boldsymbol{h}} \boldsymbol{v_H}$. Otherwise $\boldsymbol{y^0} \neq \boldsymbol{0}$, hence there is $j \in \{1, \dots, N_L\}$ with $y_j^0 \neq 0$ and thus by definition

$$k y_j^k \not\to 0.$$

This means there exists some constant $C > 0$ such that

$$\left| y_j^k \right| \geq C \frac{1}{k} \quad \text{or} \quad \left\| p_h^k \right\| \geq C \frac{1}{k}.$$

□

Remark 4.3. If $\mathcal{T}_h$ is obtained from $\mathcal{T}_H$ by uniform refinement, then we obviously have $H_H \subseteq H_h$ as well as $L_H \subseteq L_h$ and thus the L^2-projection from H_H onto H_h is the identity mapping. As a consequence, we have $\boldsymbol{P_h v_H} = \boldsymbol{v_H}$. However, in general, we have

$$(\nabla \cdot \boldsymbol{v_H}, \chi) \neq 0$$

for $\chi \in L_h \setminus L_H$ also in this case and hence $\boldsymbol{P_h v_H} \neq \widetilde{\boldsymbol{P}}_{\boldsymbol{h}} \boldsymbol{v_H}$.

In the remaining part of this section, we want to show that the pressure approximations $\hat{p}_h^k$ obtained through equation (4.5) remain bounded for $k \to 0$.

To do so we introduce some auxiliary quantities: Analog to (4.3), let the approximate solution $(\boldsymbol{v_h}, p_h)^T \in H_h^d \times L_h$ of the Stokes problem on the mesh $\mathcal{T}_h$ be given by

$$\begin{aligned} (\nabla \boldsymbol{v_h}, \nabla \boldsymbol{\psi}) - (p_h, \nabla \cdot \boldsymbol{\psi}) &= (\boldsymbol{f}, \boldsymbol{\psi}) && \forall \boldsymbol{\psi} \in H_h^d, \\ (\nabla \cdot \boldsymbol{v_h}, \chi) &= 0 && \forall \chi \in L_h. \end{aligned} \tag{4.11}$$

Then in addition to the H-projection $\widetilde{\boldsymbol{P}}_{\boldsymbol{h}} \boldsymbol{v}$ of the continuous velocity $\boldsymbol{v}$ defined by (4.6) we consider the V-projection $\widetilde{\boldsymbol{R}}_{\boldsymbol{h}} \boldsymbol{v}$ of the continuous velocity $\boldsymbol{v}$ into H_h^d. It is given as the first component of the solution $(\widetilde{\boldsymbol{R}}_{\boldsymbol{h}} \boldsymbol{v}, \tilde{r}_h)^T \in H_h^d \times L_h$ of

$$\begin{aligned} (\nabla \widetilde{\boldsymbol{R}}_{\boldsymbol{h}} \boldsymbol{v}, \nabla \boldsymbol{\psi}) - (\tilde{r}_h, \nabla \cdot \boldsymbol{\psi}) &= (\nabla \boldsymbol{v}, \nabla \boldsymbol{\psi}) && \forall \boldsymbol{\psi} \in H_h^d, \\ (\nabla \cdot \widetilde{\boldsymbol{R}}_{\boldsymbol{h}} \boldsymbol{v}, \chi) &= 0 && \forall \chi \in L_h. \end{aligned} \tag{4.12}$$

Lemma 4.4. *The pressure $\hat{p}_h^k$ obtained from* (4.5) *is bounded independent of* k.

Proof. Subtracting $\frac{1}{k}$ times the first equation of (4.6) from the first equation of (4.4) leads to

$$\frac{1}{k}(\boldsymbol{v_h^k} - \widetilde{\boldsymbol{P}}_{\boldsymbol{h}}\boldsymbol{v_H}, \boldsymbol{\psi}) + (\nabla \boldsymbol{v_h^k}, \nabla \boldsymbol{\psi}) - \frac{1}{k}(kp_h^k - \tilde{p}_h^H, \nabla \cdot \boldsymbol{\psi}) = (\boldsymbol{f}, \boldsymbol{\psi}) \quad \forall \boldsymbol{\psi} \in H_h^d$$

or equivalently

$$\begin{aligned}\frac{1}{k}(\boldsymbol{v_h^k} - \widetilde{\boldsymbol{P}}_{\boldsymbol{h}}\boldsymbol{v_H}, \boldsymbol{\psi}) + (\nabla(\boldsymbol{v_h^k} - \widetilde{\boldsymbol{P}}_{\boldsymbol{h}}\boldsymbol{v_H}), \nabla \boldsymbol{\psi}) - \frac{1}{k}(kp_h^k - \tilde{p}_h^H, \nabla \cdot \boldsymbol{\psi}) \\ = (\boldsymbol{f}, \boldsymbol{\psi}) - (\nabla \widetilde{\boldsymbol{P}}_{\boldsymbol{h}}\boldsymbol{v_H}, \nabla \boldsymbol{\psi}) \quad \forall \boldsymbol{\psi} \in H_h^d.\end{aligned}$$

By testing with $\boldsymbol{\psi} = \boldsymbol{v_h^k} - \widetilde{\boldsymbol{P}}_{\boldsymbol{h}}\boldsymbol{v_H} \in H_h^d$, we obtain

$$\begin{aligned}\frac{1}{k}\left\|\boldsymbol{v_h^k} - \widetilde{\boldsymbol{P}}_{\boldsymbol{h}}\boldsymbol{v_H}\right\|^2 + \left\|\nabla(\boldsymbol{v_h^k} - \widetilde{\boldsymbol{P}}_{\boldsymbol{h}}\boldsymbol{v_H})\right\|^2 \\ = (\boldsymbol{f}, \boldsymbol{v_h^k} - \widetilde{\boldsymbol{P}}_{\boldsymbol{h}}\boldsymbol{v_H}) - (\nabla \widetilde{\boldsymbol{P}}_{\boldsymbol{h}}\boldsymbol{v_H}, \nabla(\boldsymbol{v_h^k} - \widetilde{\boldsymbol{P}}_{\boldsymbol{h}}\boldsymbol{v_H})),\end{aligned} \tag{4.13}$$

because the other terms cancel out due to the second equations of (4.4) and (4.6).

We then have for arbitrary $\boldsymbol{\psi} \in H_h^d$

$$\begin{aligned}\left|(\nabla \widetilde{\boldsymbol{P}}_{\boldsymbol{h}}\boldsymbol{v_H}, \nabla \boldsymbol{\psi})\right| = \ & \left|(\nabla(\widetilde{\boldsymbol{P}}_{\boldsymbol{h}}\boldsymbol{v_H} - \widetilde{\boldsymbol{R}}_{\boldsymbol{h}}\boldsymbol{v}), \nabla \boldsymbol{\psi})\right. \\ & \left. +(\nabla(\widetilde{\boldsymbol{R}}_{\boldsymbol{h}}\boldsymbol{v} - \boldsymbol{v}), \nabla \boldsymbol{\psi}) + (\nabla \boldsymbol{v}, \nabla \boldsymbol{\psi})\right| \\ \leq \ & \left\{\left\|\nabla(\widetilde{\boldsymbol{P}}_{\boldsymbol{h}}\boldsymbol{v_H} - \widetilde{\boldsymbol{R}}_{\boldsymbol{h}}\boldsymbol{v})\right\|\right. \\ & \left. + \left\|\nabla(\widetilde{\boldsymbol{R}}_{\boldsymbol{h}}\boldsymbol{v} - \boldsymbol{v})\right\|\right\} \|\nabla \boldsymbol{\psi}\| + \left|(\Delta \boldsymbol{v}, \boldsymbol{\psi})\right| \\ \leq \ & C\Big\{h^{-2}\left\|\widetilde{\boldsymbol{P}}_{\boldsymbol{h}}\boldsymbol{v_H} - \widetilde{\boldsymbol{R}}_{\boldsymbol{h}}\boldsymbol{v}\right\| \\ & + h^{-1}\left\|\nabla(\widetilde{\boldsymbol{R}}_{\boldsymbol{h}}\boldsymbol{v} - \boldsymbol{v})\right\| + \|\Delta \boldsymbol{v}\|\Big\} \|\boldsymbol{\psi}\| \\ \leq \ & Ch^{-2}\Big\{\left\|\widetilde{\boldsymbol{P}}_{\boldsymbol{h}}\boldsymbol{v_H} - \widetilde{\boldsymbol{P}}_{\boldsymbol{h}}\boldsymbol{v}\right\| + \left\|\widetilde{\boldsymbol{P}}_{\boldsymbol{h}}\boldsymbol{v} - \boldsymbol{v}\right\| \\ & + \left\|\boldsymbol{v} - \widetilde{\boldsymbol{R}}_{\boldsymbol{h}}\boldsymbol{v}\right\| + h\left\|\nabla(\widetilde{\boldsymbol{R}}_{\boldsymbol{h}}\boldsymbol{v} - \boldsymbol{v})\right\| \\ & + h^2\|\Delta \boldsymbol{v}\|\Big\} \|\boldsymbol{\psi}\|,\end{aligned} \tag{4.14}$$

where in the penultimate line inverse estimates have been used. We will now treat each term separately.

By subtracting the H-Projection of $\boldsymbol{v}$ from (4.6), we obtain

$$\begin{aligned}(\widetilde{\boldsymbol{P}}_{\boldsymbol{h}}\boldsymbol{v_H} - \widetilde{\boldsymbol{P}}_{\boldsymbol{h}}\boldsymbol{v}, \boldsymbol{\psi}) - (\tilde{p}_h^H - \tilde{p}_h, \nabla \cdot \boldsymbol{\psi}) = (\boldsymbol{v_H} - \boldsymbol{v}, \boldsymbol{\psi}) \qquad & \forall \boldsymbol{\psi} \in H_h^d, \\ (\nabla \cdot (\widetilde{\boldsymbol{P}}_{\boldsymbol{h}}\boldsymbol{v_H} - \widetilde{\boldsymbol{P}}_{\boldsymbol{h}}\boldsymbol{v}), \chi) = 0 \qquad & \forall \chi \in L_h.\end{aligned} \tag{4.15}$$

Testing with $\boldsymbol{\psi} \coloneqq \widetilde{\boldsymbol{P}}_{\boldsymbol{h}}\boldsymbol{v}_{\boldsymbol{H}} - \widetilde{\boldsymbol{P}}_{\boldsymbol{h}}\boldsymbol{v}$ and $\chi \coloneqq \tilde{p}_h^H - \tilde{p}_h$ yields

$$\left\|\widetilde{\boldsymbol{P}}_{\boldsymbol{h}}\boldsymbol{v}_{\boldsymbol{H}} - \widetilde{\boldsymbol{P}}_{\boldsymbol{h}}\boldsymbol{v}\right\|^2 = (\boldsymbol{v}_{\boldsymbol{H}} - \boldsymbol{v}, \widetilde{\boldsymbol{P}}_{\boldsymbol{h}}\boldsymbol{v}_{\boldsymbol{H}} - \widetilde{\boldsymbol{P}}_{\boldsymbol{h}}\boldsymbol{v})$$

and hence due to the Cauchy-Schwarz inequality

$$\left\|\widetilde{\boldsymbol{P}}_{\boldsymbol{h}}\boldsymbol{v}_{\boldsymbol{H}} - \widetilde{\boldsymbol{P}}_{\boldsymbol{h}}\boldsymbol{v}\right\| \leq \|\boldsymbol{v}_{\boldsymbol{H}} - \boldsymbol{v}\|.$$

Using standard approximation results (see, for instance, [17]) and the a priori estimate (4.2), we obtain

$$\left\|\widetilde{\boldsymbol{P}}_{\boldsymbol{h}}\boldsymbol{v}_{\boldsymbol{H}} - \widetilde{\boldsymbol{P}}_{\boldsymbol{h}}\boldsymbol{v}\right\| \leq \|\boldsymbol{v} - \boldsymbol{v}_{\boldsymbol{H}}\| \leq CH^2\left\{\|\boldsymbol{v}\|_{H^2} + \|p\|_{H^1}\right\} \leq CH^2\|\boldsymbol{f}\|. \quad (4.16)$$

In order to estimate the next term, we note that from (4.6) we have

$$(\widetilde{\boldsymbol{P}}_{\boldsymbol{h}}\boldsymbol{v} - \boldsymbol{v}, \boldsymbol{\psi}) = (\tilde{p}_h, \nabla \cdot \boldsymbol{\psi}) \quad \forall \boldsymbol{\psi} \in H_h^d.$$

Testing with $\boldsymbol{\psi} \coloneqq \boldsymbol{v}_{\boldsymbol{h}} - \widetilde{\boldsymbol{P}}_{\boldsymbol{h}}\boldsymbol{v}$ and recalling that

$$(\nabla \cdot \boldsymbol{v}_{\boldsymbol{h}}, \chi) = (\nabla \cdot \widetilde{\boldsymbol{P}}_{\boldsymbol{h}}\boldsymbol{v}, \chi) = 0 \quad \forall \chi \in L_h,$$

we conclude

$$(\widetilde{\boldsymbol{P}}_{\boldsymbol{h}}\boldsymbol{v} - \boldsymbol{v}, \boldsymbol{v}_{\boldsymbol{h}} - \widetilde{\boldsymbol{P}}_{\boldsymbol{h}}\boldsymbol{v}) = (\tilde{p}_h, \nabla \cdot (\boldsymbol{v}_{\boldsymbol{h}} - \widetilde{\boldsymbol{P}}_{\boldsymbol{h}}\boldsymbol{v})) = 0.$$

Thus, we have

$$\left\|\widetilde{\boldsymbol{P}}_{\boldsymbol{h}}\boldsymbol{v} - \boldsymbol{v}\right\|^2 = (\widetilde{\boldsymbol{P}}_{\boldsymbol{h}}\boldsymbol{v} - \boldsymbol{v}, \widetilde{\boldsymbol{P}}_{\boldsymbol{h}}\boldsymbol{v} - \boldsymbol{v}) = (\widetilde{\boldsymbol{P}}_{\boldsymbol{h}}\boldsymbol{v} - \boldsymbol{v}, \boldsymbol{v}_{\boldsymbol{h}} - \boldsymbol{v}) \leq \left\|\widetilde{\boldsymbol{P}}_{\boldsymbol{h}}\boldsymbol{v} - \boldsymbol{v}\right\| \|\boldsymbol{v}_{\boldsymbol{h}} - \boldsymbol{v}\|$$

and therefore

$$\left\|\widetilde{\boldsymbol{P}}_{\boldsymbol{h}}\boldsymbol{v} - \boldsymbol{v}\right\| \leq \|\boldsymbol{v} - \boldsymbol{v}_{\boldsymbol{h}}\| \leq Ch^2\|\boldsymbol{f}\|. \quad (4.17)$$

Similarly, from (4.12) we see that

$$(\nabla(\widetilde{\boldsymbol{R}}_{\boldsymbol{h}}\boldsymbol{v} - \boldsymbol{v}), \nabla\boldsymbol{\psi}) = (\tilde{r}_h, \nabla \cdot \boldsymbol{\psi}) \quad \forall \boldsymbol{\psi} \in H_h^d \quad (4.18)$$

and hence by testing with $\boldsymbol{\psi} \coloneqq \boldsymbol{v}_{\boldsymbol{h}} - \widetilde{\boldsymbol{R}}_{\boldsymbol{h}}\boldsymbol{v}$

$$(\nabla(\widetilde{\boldsymbol{R}}_{\boldsymbol{h}}\boldsymbol{v} - \boldsymbol{v}), \nabla(\boldsymbol{v}_{\boldsymbol{h}} - \widetilde{\boldsymbol{R}}_{\boldsymbol{h}}\boldsymbol{v})) = (\tilde{r}_h, \nabla \cdot (\boldsymbol{v}_{\boldsymbol{h}} - \widetilde{\boldsymbol{R}}_{\boldsymbol{h}}\boldsymbol{v})) = 0.$$

This yields

$$\begin{aligned}\left\|\nabla(\widetilde{\boldsymbol{R}}_{\boldsymbol{h}}\boldsymbol{v} - \boldsymbol{v})\right\|^2 &= (\nabla(\widetilde{\boldsymbol{R}}_{\boldsymbol{h}}\boldsymbol{v} - \boldsymbol{v}), \nabla(\widetilde{\boldsymbol{R}}_{\boldsymbol{h}}\boldsymbol{v} - \boldsymbol{v})) = (\nabla(\widetilde{\boldsymbol{R}}_{\boldsymbol{h}}\boldsymbol{v} - \boldsymbol{v}), \nabla(\boldsymbol{v}_{\boldsymbol{h}} - \boldsymbol{v})) \\ &\leq \left\|\nabla(\widetilde{\boldsymbol{R}}_{\boldsymbol{h}}\boldsymbol{v} - \boldsymbol{v})\right\| \left\|\nabla(\boldsymbol{v}_{\boldsymbol{h}} - \boldsymbol{v})\right\|\end{aligned}$$

and thus

$$\left\|\nabla(\widetilde{\boldsymbol{R}}_{\boldsymbol{h}}\boldsymbol{v} - \boldsymbol{v})\right\| \leq \left\|\nabla(\boldsymbol{v} - \boldsymbol{v}_{\boldsymbol{h}})\right\| \leq Ch\|\boldsymbol{f}\|. \quad (4.19)$$

Before estimating $\left\|\widetilde{\boldsymbol{R}}_{\boldsymbol{h}}\boldsymbol{v}-\boldsymbol{v}\right\|$, we recall equations (4.18) and (4.19) as well as the inf-sup stability condition (2.1) which allows us to bound $\|\tilde{r}_h\|$:

$$\begin{aligned}\beta\left\|\tilde{r}_h\right\| &\leq \sup_{\boldsymbol{\psi}\in H_h^d}\frac{(\tilde{r}_h,\nabla\cdot\boldsymbol{\psi})}{\|\nabla\boldsymbol{\psi}\|}\\ &= \sup_{\boldsymbol{\psi}\in H_h^d}\frac{(\nabla(\widetilde{\boldsymbol{R}}_{\boldsymbol{h}}\boldsymbol{v}-\boldsymbol{v}),\nabla\boldsymbol{\psi})}{\|\nabla\boldsymbol{\psi}\|}\leq\left\|\nabla(\widetilde{\boldsymbol{R}}_{\boldsymbol{h}}\boldsymbol{v}-\boldsymbol{v})\right\|\leq Ch\left\|\boldsymbol{f}\right\|.\end{aligned}\tag{4.20}$$

In order to estimate $\left\|\widetilde{\boldsymbol{R}}_{\boldsymbol{h}}\boldsymbol{v}-\boldsymbol{v}\right\|$, we use a duality argument due to [1] and [27]: Let $(\boldsymbol{w},q)^T\in H_0^1(\Omega)^d\times L^2(\Omega)/\mathbb{R}$ be the unique solution of

$$\begin{aligned}(\nabla\boldsymbol{\psi},\nabla\boldsymbol{w})+(\nabla\cdot\boldsymbol{\psi},q)&=\frac{(\boldsymbol{\psi},\boldsymbol{v}-\widetilde{\boldsymbol{R}}_{\boldsymbol{h}}\boldsymbol{v})}{\left\|\boldsymbol{v}-\widetilde{\boldsymbol{R}}_{\boldsymbol{h}}\boldsymbol{v}\right\|}\qquad&&\forall\boldsymbol{\psi}\in H_0^1(\Omega)^d,\\ -(\chi,\nabla\cdot\boldsymbol{w})&=0&&\forall\chi\in L^2(\Omega)/\mathbb{R}.\end{aligned}\tag{4.21}$$

Since $\frac{\boldsymbol{v}-\widetilde{\boldsymbol{R}}_{\boldsymbol{h}}\boldsymbol{v}}{\|\boldsymbol{v}-\widetilde{\boldsymbol{R}}_{\boldsymbol{h}}\boldsymbol{v}\|}\in L^2(\Omega)^d$, we have as for the primal problem (4.1) the a priori estimate

$$\left\|\boldsymbol{w}\right\|_{H^2}+\left\|q\right\|_{H^1}\leq C\left\|\tfrac{\boldsymbol{v}-\widetilde{\boldsymbol{R}}_{\boldsymbol{h}}\boldsymbol{v}}{\|\boldsymbol{v}-\widetilde{\boldsymbol{R}}_{\boldsymbol{h}}\boldsymbol{v}\|}\right\|=C.\tag{4.22}$$

Testing the first equation of (4.21) with $\boldsymbol{v}-\widetilde{\boldsymbol{R}}_{\boldsymbol{h}}\boldsymbol{v}\in H_0^1(\Omega)^d$, we obtain

$$\left\|\boldsymbol{v}-\widetilde{\boldsymbol{R}}_{\boldsymbol{h}}\boldsymbol{v}\right\|=(\nabla(\boldsymbol{v}-\widetilde{\boldsymbol{R}}_{\boldsymbol{h}}\boldsymbol{v}),\nabla\boldsymbol{w})+(\nabla\cdot(\boldsymbol{v}-\widetilde{\boldsymbol{R}}_{\boldsymbol{h}}\boldsymbol{v}),q).$$

Recalling (4.18) and the fact that

$$(\nabla\cdot\boldsymbol{v},\chi)=(\nabla\cdot\boldsymbol{w},\chi)=(\nabla\cdot\widetilde{\boldsymbol{R}}_{\boldsymbol{h}}\boldsymbol{v},\chi)=0\quad\forall\chi\in L_h,$$

we may write for arbitrary $\hat{\boldsymbol{w}}_{\boldsymbol{h}}\in H_h^d$ and $\hat{q}_h\in L_h$

$$\begin{aligned}\left\|\boldsymbol{v}-\widetilde{\boldsymbol{R}}_{\boldsymbol{h}}\boldsymbol{v}\right\|&=(\nabla(\boldsymbol{v}-\widetilde{\boldsymbol{R}}_{\boldsymbol{h}}\boldsymbol{v}),\nabla(\boldsymbol{w}-\hat{\boldsymbol{w}}_{\boldsymbol{h}})\\ &\quad+(\nabla\cdot(\boldsymbol{v}-\widetilde{\boldsymbol{R}}_{\boldsymbol{h}}\boldsymbol{v}),q-\hat{q}_h)-(\tilde{r}_h,\nabla\cdot(\boldsymbol{w}-\hat{\boldsymbol{w}}_{\boldsymbol{h}}))\\ &\leq C\Big\{\left\|\nabla(\boldsymbol{v}-\widetilde{\boldsymbol{R}}_{\boldsymbol{h}}\boldsymbol{v})\right\|+\left\|\tilde{r}_h\right\|\Big\}\big\{\left\|\nabla(\boldsymbol{w}-\hat{\boldsymbol{w}}_{\boldsymbol{h}})\right\|+\left\|q-\hat{q}_h\right\|\big\}.\end{aligned}$$

From standard interpolation estimates, see, e. g., [6, 11] we obtain

$$\begin{aligned}\left\|\nabla(\boldsymbol{w}-\hat{\boldsymbol{w}}_{\boldsymbol{h}})\right\|&\leq Ch\left\|\boldsymbol{w}\right\|_{H^2},\\ \left\|q-\hat{q}_h\right\|&\leq Ch\left\|q\right\|_{H^1}.\end{aligned}$$

Together with the estimates (4.19) and (4.20), we have

$$\left\|\boldsymbol{v}-\widetilde{\boldsymbol{R}}_{\boldsymbol{h}}\boldsymbol{v}\right\|\leq Ch^2\left\|\boldsymbol{f}\right\|\left\{\left\|\boldsymbol{w}\right\|_{H^2}+\left\|q\right\|_{H^1}\right\}\leq Ch^2\left\|\boldsymbol{f}\right\|,\tag{4.23}$$

where the last inequality is obtained by applying the a priori estimate (4.22). Finally, we obviously have

$$\left\|\Delta\boldsymbol{v}\right\|\leq\left\|\boldsymbol{v}\right\|_{H^2}\leq C\left\|\boldsymbol{f}\right\|.\tag{4.24}$$

Inserting the estimates (4.16), (4.17), (4.19), (4.23), and (4.24) into (4.14) then yields

$$\left|(\nabla \widetilde{\boldsymbol{P}}_{\boldsymbol{h}} \boldsymbol{v}_{\boldsymbol{H}}, \nabla \boldsymbol{\psi})\right| \leq C\big(1 + (\tfrac{H}{h})^2\big) \, \|\boldsymbol{f}\| \, \|\boldsymbol{\psi}\| \, .$$

Since we only consider uniform refinement or uniform coarsening, we have $H = 2h$ or $H = \frac{1}{2}h$ and thus

$$\left|(\nabla \widetilde{\boldsymbol{P}}_{\boldsymbol{h}} \boldsymbol{v}_{\boldsymbol{H}}, \nabla \boldsymbol{\psi})\right| \leq C \, \|\boldsymbol{f}\| \, \|\boldsymbol{\psi}\| \, . \tag{4.25}$$

This allows us to conclude from (4.13):

$$\begin{aligned} \frac{1}{k} \left\| \boldsymbol{v}_{\boldsymbol{h}}^{\boldsymbol{k}} - \widetilde{\boldsymbol{P}}_{\boldsymbol{h}} \boldsymbol{v}_{\boldsymbol{H}} \right\|^2 + \left\| \nabla (\boldsymbol{v}_{\boldsymbol{h}}^{\boldsymbol{k}} - \widetilde{\boldsymbol{P}}_{\boldsymbol{h}} \boldsymbol{v}_{\boldsymbol{H}}) \right\|^2 &\leq \|\boldsymbol{f}\| \left\| \boldsymbol{v}_{\boldsymbol{h}}^{\boldsymbol{k}} - \widetilde{\boldsymbol{P}}_{\boldsymbol{h}} \boldsymbol{v}_{\boldsymbol{H}} \right\| \\ &\quad + \left| (\nabla \widetilde{\boldsymbol{P}}_{\boldsymbol{h}} \boldsymbol{v}_{\boldsymbol{H}}, \nabla (\boldsymbol{v}_{\boldsymbol{h}}^{\boldsymbol{k}} - \widetilde{\boldsymbol{P}}_{\boldsymbol{h}} \boldsymbol{v}_{\boldsymbol{H}})) \right| \\ &\leq C \, \|\boldsymbol{f}\| \left\| \boldsymbol{v}_{\boldsymbol{h}}^{\boldsymbol{k}} - \widetilde{\boldsymbol{P}}_{\boldsymbol{h}} \boldsymbol{v}_{\boldsymbol{H}} \right\| \end{aligned}$$

and hence

$$\frac{1}{k} \left\| \boldsymbol{v}_{\boldsymbol{h}}^{\boldsymbol{k}} - \widetilde{\boldsymbol{P}}_{\boldsymbol{h}} \boldsymbol{v}_{\boldsymbol{H}} \right\| \leq C \, \|\boldsymbol{f}\| \, . \tag{4.26}$$

By using the Poincaré inequality, we also obtain from (4.25)

$$\left|(\nabla \widetilde{\boldsymbol{P}}_{\boldsymbol{h}} \boldsymbol{v}_{\boldsymbol{H}}, \nabla \boldsymbol{\psi})\right| \leq C \, \|\boldsymbol{f}\| \, \|\nabla \boldsymbol{\psi}\| \tag{4.27}$$

and therefore from (4.13) also

$$\left\| \nabla (\boldsymbol{v}_{\boldsymbol{h}}^{\boldsymbol{k}} - \widetilde{\boldsymbol{P}}_{\boldsymbol{h}} \boldsymbol{v}_{\boldsymbol{H}}) \right\| \leq C \, \|\boldsymbol{f}\| \, . \tag{4.28}$$

To show that $\left\|\hat{p}_h^k\right\|$ remains bounded for $k \to 0$, we use the inf-sup condition and the fact that $\boldsymbol{v}_{\boldsymbol{h}}^{\boldsymbol{k}} = \hat{\boldsymbol{v}}_{\boldsymbol{h}}^{\boldsymbol{k}}$ which allows us to replace $\hat{\boldsymbol{v}}_{\boldsymbol{h}}^{\boldsymbol{k}}$ by $\boldsymbol{v}_{\boldsymbol{h}}^{\boldsymbol{k}}$ in (4.5):

$$\begin{aligned} \beta \left\| \hat{p}_h^k \right\| &\leq \sup_{\boldsymbol{\psi} \in H_h^d} \frac{(\hat{p}_h^k, \nabla \cdot \boldsymbol{\psi})}{\|\nabla \boldsymbol{\psi}\|} \\ &= \sup_{\boldsymbol{\psi} \in H_h^d} \left(\frac{\frac{1}{k} (\boldsymbol{v}_{\boldsymbol{h}}^{\boldsymbol{k}} - \widetilde{\boldsymbol{P}}_{\boldsymbol{h}} \boldsymbol{v}_{\boldsymbol{H}}, \boldsymbol{\psi}) + (\nabla (\boldsymbol{v}_{\boldsymbol{h}}^{\boldsymbol{k}} - \widetilde{\boldsymbol{P}}_{\boldsymbol{h}} \boldsymbol{v}_{\boldsymbol{H}}), \nabla \boldsymbol{\psi})}{\|\nabla \boldsymbol{\psi}\|} \right. \\ &\qquad \left. + \frac{(\nabla \widetilde{\boldsymbol{P}}_{\boldsymbol{h}} \boldsymbol{v}_{\boldsymbol{H}}, \nabla \boldsymbol{\psi}) - (\boldsymbol{f}, \boldsymbol{\psi})}{\|\nabla \boldsymbol{\psi}\|} \right) \\ &\leq C \frac{1}{k} \left\| \boldsymbol{v}_{\boldsymbol{h}}^{\boldsymbol{k}} - \widetilde{\boldsymbol{P}}_{\boldsymbol{h}} \boldsymbol{v}_{\boldsymbol{H}} \right\| + \left\| \nabla (\boldsymbol{v}_{\boldsymbol{h}}^{\boldsymbol{k}} - \widetilde{\boldsymbol{P}}_{\boldsymbol{h}} \boldsymbol{v}_{\boldsymbol{H}}) \right\| \\ &\quad + \sup_{\boldsymbol{\psi} \in H_h^d} \frac{\left| (\nabla \widetilde{\boldsymbol{P}}_{\boldsymbol{h}} \boldsymbol{v}_{\boldsymbol{H}}, \nabla \boldsymbol{\psi}) \right|}{\|\nabla \boldsymbol{\psi}\|} + C \, \|\boldsymbol{f}\| \\ &\leq C \, \|\boldsymbol{f}\| \, . \end{aligned}$$

Here, the estimates (4.26), (4.27), and (4.28) have been used. Since the right-hand side is independent of k, we have shown that $\left\|\hat{p}_h^k\right\|$ remains bounded for $k \to 0$. □

Remark 4.5. The arguments used above to show that $\left\|p_h^k\right\| \geq C\frac{1}{k}$ if there is a $\chi \in L_h$ such that $(\nabla \cdot \boldsymbol{P_h v_H}, \chi) \neq 0$ are not restricted to the case of uniform refinement or coarsening of the meshes. Actually, they directly carry over to the case of arbitrary refinement or coarsening of cells. The estimate for the boundedness of $\left\|\hat{p}_h^k\right\|$ can be generalized as long we are able to bound $\left\|\nabla \widetilde{\boldsymbol{P}}_{\boldsymbol{h}} \boldsymbol{v_H}\right\|$ and $\left\|\tilde{\Delta}_h \widetilde{\boldsymbol{P}}_{\boldsymbol{h}} \boldsymbol{v_H}\right\|$ where $\tilde{\Delta}_h \widetilde{\boldsymbol{P}}_{\boldsymbol{h}} \boldsymbol{v_H}$ denotes the discrete Stokes operator of $\widetilde{\boldsymbol{P}}_{\boldsymbol{h}} \boldsymbol{v_H}$ given by

$$(\tilde{\Delta}_h \widetilde{\boldsymbol{P}}_{\boldsymbol{h}} \boldsymbol{v_H}, \boldsymbol{\psi}) = -(\nabla \widetilde{\boldsymbol{P}}_{\boldsymbol{h}} \boldsymbol{v_H}, \nabla \boldsymbol{\psi}) \qquad \forall \boldsymbol{\psi} \in H_h^d \cap \left\{ \boldsymbol{\psi} \;\middle|\; (\nabla \cdot \boldsymbol{\psi}, \chi) = 0 \ \forall \chi \in L_h \right\}.$$

We showed that on dynamic spatial meshes bounded pressure approximations are only possible if the L^2-projection of the velocity from the first mesh is divergence-free with respect to the test functions of the new mesh. Otherwise, the pressure approximation contains $\frac{1}{k}$ times the Lagrange multiplier occurring in the H-projection of the old velocity field into the new finite element space which leads to the unbounded behavior for $k \to 0$.

5. Solution of the problem

The following Subsection 5.1 presents some attempts to solve the problem discussed in this article.

5.1. Attempts to solve this problem

We have seen in the previous section that the error in the pressure occurring when switching the spatial mesh decreases with (at least) the same order as the spatial discretization error for $h \to 0$, but increases like $O(k^{-1})$ for $k \to 0$. We showed that this effect does not originate from the stabilization since the inf-sup-stable Taylor-Hood element also produces qualitatively the same error. In this subsection, we discuss some attempts to overcome this problem and obtain pressure approximations which remain bounded for $k \to 0$.

We also showed analytically that the error in the pressure approximation which is solely located in the first time step on a new spatial mesh is unavoidable if the L^2-projection of the old velocity field is not divergence-free with respect to test functions of the new finite element space for the pressure. However, the proposed approach to solving this problem namely taking the divergence-free L^2-projection as initial values on the new spatial mesh might be too costly to perform each time the mesh is changed. Therefore, we present two alternatives to the H-projection that might be easier to implement or less costly which might be able to deal with this phenomenon, too. To sum up, the three "ideas" discussed in this section are:

Divergence-free L^2-projection (H-projection):.
After computing $(\boldsymbol{V_{m-1}}, P_{m-1})^T \in (H_h^{m-1})^d \times L_h^{m-1}$ first compute a projection $\widetilde{\boldsymbol{V}}_{\boldsymbol{m-1}}$ of $\boldsymbol{V_{m-1}}$ into $(H_h^m)^d$ which is divergence-free with

TABLE 7. $\|p - p_{kh}\|$ for the cG(1) discretization with different temporal discretizations and H-projection

level	dG(0)		dG(1)		fractional-step-θ	
	$t = 3 + k$	$t = 6 + k$	$t = 3 + k$	$t = 6 + k$	$t = 3 + k$	$t = 6 + k$
1	$3.47 \cdot 10^{-2}$	$1.27 \cdot 10^{-1}$	$3.77 \cdot 10^{-2}$	$1.28 \cdot 10^{-1}$	$3.08 \cdot 10^{-2}$	$1.25 \cdot 10^{-1}$
2	$3.42 \cdot 10^{-2}$	$1.25 \cdot 10^{-1}$	$3.51 \cdot 10^{-2}$	$1.25 \cdot 10^{-1}$	$3.12 \cdot 10^{-2}$	$1.24 \cdot 10^{-1}$
3	$3.48 \cdot 10^{-2}$	$1.24 \cdot 10^{-1}$	$3.49 \cdot 10^{-2}$	$1.24 \cdot 10^{-1}$	$3.28 \cdot 10^{-2}$	$1.24 \cdot 10^{-1}$
4	$3.57 \cdot 10^{-2}$	$1.24 \cdot 10^{-1}$	$3.57 \cdot 10^{-2}$	$1.24 \cdot 10^{-1}$	$3.42 \cdot 10^{-2}$	$1.24 \cdot 10^{-1}$
order	-0.04	0.00	-0.03	0.00	-0.06	0.00

respect to test functions in $(H_h^m)^d$ and use this projection as initial values for the next time step. The projection is determined by

$$\begin{aligned} (\widetilde{\boldsymbol{V}}_{\boldsymbol{m-1}}, \boldsymbol{\psi}) - (\widetilde{P}, \nabla \cdot \boldsymbol{\psi}) &= (\boldsymbol{V}_{\boldsymbol{m-1}}, \boldsymbol{\psi}) && \forall \boldsymbol{\psi} \in (H_h^m)^d, \\ (\nabla \cdot \widetilde{\boldsymbol{V}}_{\boldsymbol{m-1}}, \chi) &= 0 && \forall \chi \in L_h^m. \end{aligned} \tag{5.1}$$

Divergence-free $\boldsymbol{H_0^1}$-projection ($\boldsymbol{V}$-projection):.
Same procedure as for "Divergence-free L^2-projection", but this time the projection is determined by

$$\begin{aligned} (\nabla \widetilde{\boldsymbol{V}}_{\boldsymbol{m-1}}, \nabla \boldsymbol{\psi}) - (\widetilde{P}, \nabla \cdot \boldsymbol{\psi}) &= (\nabla \boldsymbol{V}_{\boldsymbol{m-1}}, \nabla \boldsymbol{\psi}) && \forall \boldsymbol{\psi} \in (H_h^m)^d, \\ (\nabla \cdot \widetilde{\boldsymbol{V}}_{\boldsymbol{m-1}}, \chi) &= 0 && \forall \chi \in L_h^m. \end{aligned} \tag{5.2}$$

Repeating one time step:.
After computing $(\boldsymbol{V}_{\boldsymbol{m-1}}, P_{m-1})^T \in (H_h^{m-1})^d \times L_h^{m-1}$ repeat the current time step to determine approximations $(\widetilde{\boldsymbol{V}}_{\boldsymbol{m-1}}, \widetilde{P}_{m-1})^T \in (H_h^m)^d \times L_h^m$ for $t = t_{m-1}$, but already in the finite element spaces corresponding to $t = t_m$. One can hope that then only $\widetilde{P}_{m-1}$ contains this error and since $\widetilde{\boldsymbol{V}}_{\boldsymbol{m-1}}$ is divergence-free with respect to test functions in L_h^m this error does not occur again when computing $(\boldsymbol{V}_{\boldsymbol{m}}, P_m)^T \in (H_h^m)^d \times L_h^m$ using the initial values $\widetilde{\boldsymbol{V}}_{\boldsymbol{m-1}}$.

For the equal-order spatial discretizations cG(1) and cG(2) the variational formulations given above have to be stabilized, of course. This is also done by means of the local projection stabilization.

Since the behavior of the pressure error already is of the right order for $h \to 0$, we discuss in this subsection only the influence of the presented "ideas" on the development of the error under uniform temporal refinement. We repeat the investigation of Section 4.1.2 using the proposed modifications.

5.1.1. $\boldsymbol{H}$-projection. In this subsection, we present the development of the pressure error when using the H-projection of the old velocity field into the new finite element space as initial values when switching the spatial mesh.

The results under uniform temporal refinement are listed in Tables 7–9 for the cG(1), cG(2), and $\mathcal{Q}_2/\mathcal{Q}_1$ spatial discretization, respectively.

TABLE 8. $\|p - p_{kh}\|$ for the cG(2) discretization with different temporal discretizations and H-projection

level	dG(0)		dG(1)		fractional-step-θ	
	$t = 3 + k$	$t = 6 + k$	$t = 3 + k$	$t = 6 + k$	$t = 3 + k$	$t = 6 + k$
1	$5.73 \cdot 10^{-3}$	$1.48 \cdot 10^{-2}$	$5.54 \cdot 10^{-3}$	$1.30 \cdot 10^{-2}$	$5.29 \cdot 10^{-3}$	$1.27 \cdot 10^{-2}$
2	$6.97 \cdot 10^{-3}$	$1.73 \cdot 10^{-2}$	$7.82 \cdot 10^{-3}$	$1.59 \cdot 10^{-2}$	$7.81 \cdot 10^{-3}$	$1.64 \cdot 10^{-2}$
3	$7.67 \cdot 10^{-3}$	$1.99 \cdot 10^{-2}$	$8.72 \cdot 10^{-3}$	$1.93 \cdot 10^{-2}$	$8.64 \cdot 10^{-3}$	$1.98 \cdot 10^{-2}$
4	$7.69 \cdot 10^{-3}$	$2.19 \cdot 10^{-2}$	$8.36 \cdot 10^{-3}$	$2.17 \cdot 10^{-2}$	$8.24 \cdot 10^{-3}$	$2.20 \cdot 10^{-2}$
order	0.00	−0.14	0.06	−0.17	0.07	−0.15

TABLE 9. $\|p - p_{kh}\|$ for the $\mathcal{Q}_2/\mathcal{Q}_1$ discretization with different temporal discretizations and H-projection

level	dG(0)		dG(1)		fractional-step-θ	
	$t = 3 + k$	$t = 6 + k$	$t = 3 + k$	$t = 6 + k$	$t = 3 + k$	$t = 6 + k$
1	$6.44 \cdot 10^{-3}$	$1.03 \cdot 10^{-2}$	$4.74 \cdot 10^{-3}$	$9.63 \cdot 10^{-3}$	$5.23 \cdot 10^{-3}$	$9.83 \cdot 10^{-3}$
2	$8.48 \cdot 10^{-3}$	$1.12 \cdot 10^{-2}$	$7.79 \cdot 10^{-3}$	$1.08 \cdot 10^{-2}$	$8.27 \cdot 10^{-3}$	$1.10 \cdot 10^{-2}$
3	$1.02 \cdot 10^{-2}$	$1.21 \cdot 10^{-2}$	$1.01 \cdot 10^{-2}$	$1.19 \cdot 10^{-2}$	$1.04 \cdot 10^{-2}$	$1.20 \cdot 10^{-2}$
4	$1.13 \cdot 10^{-2}$	$1.27 \cdot 10^{-2}$	$1.13 \cdot 10^{-2}$	$1.26 \cdot 10^{-2}$	$1.14 \cdot 10^{-2}$	$1.27 \cdot 10^{-2}$
order	−0.15	−0.07	−0.16	−0.08	−0.13	−0.08

TABLE 10. $\|p - p_{kh}\|$ for the cG(1) discretization with different temporal discretizations and V-projection

level	dG(0)		dG(1)		fractional-step-θ	
	$t = 3 + k$	$t = 6 + k$	$t = 3 + k$	$t = 6 + k$	$t = 3 + k$	$t = 6 + k$
1	$1.18 \cdot 10^{-1}$	$1.47 \cdot 10^{-1}$	$7.23 \cdot 10^{-2}$	$1.47 \cdot 10^{-1}$	$8.35 \cdot 10^{-2}$	$1.24 \cdot 10^{-1}$
2	$1.59 \cdot 10^{-1}$	$1.47 \cdot 10^{-1}$	$1.32 \cdot 10^{-1}$	$1.47 \cdot 10^{-1}$	$1.33 \cdot 10^{-1}$	$1.24 \cdot 10^{-1}$
3	$1.99 \cdot 10^{-1}$	$1.47 \cdot 10^{-1}$	$1.87 \cdot 10^{-1}$	$1.47 \cdot 10^{-1}$	$1.73 \cdot 10^{-1}$	$1.24 \cdot 10^{-1}$
4	$2.28 \cdot 10^{-1}$	$1.47 \cdot 10^{-1}$	$2.24 \cdot 10^{-1}$	$1.47 \cdot 10^{-1}$	$1.99 \cdot 10^{-1}$	$1.24 \cdot 10^{-1}$
order	−0.20	0.00	−0.26	0.00	−0.20	0.00

We can conclude that using the H-projection of the velocity of the last time step into the new finite element space as initial values leads to pressure errors which are bounded for $k \to 0$ as predicted by our analysis in Section 4.2. Actually, the pressure error becomes almost independent of k.

5.1.2. V-projection. In this subsection, we present the development of the pressure error when using the V-projection of the old velocity field into the new finite element space as initial values when switching the spatial mesh.

The results under uniform temporal refinement are listed in Tables 10–12 for the cG(1), cG(2), and $\mathcal{Q}_2/\mathcal{Q}_1$ spatial discretization, respectively.

Using the V-projection of the old velocity into the new finite element space also leads to pressure errors which remain bounded for $k \to 0$.

TABLE 11. $\|p - p_{kh}\|$ for the cG(2) discretization with different temporal discretizations and V-projection

level	dG(0)		dG(1)		fractional-step-θ	
	$t = 3 + k$	$t = 6 + k$	$t = 3 + k$	$t = 6 + k$	$t = 3 + k$	$t = 6 + k$
1	$6.08 \cdot 10^{-3}$	$1.20 \cdot 10^{-2}$	$4.86 \cdot 10^{-3}$	$1.19 \cdot 10^{-2}$	$4.90 \cdot 10^{-3}$	$9.98 \cdot 10^{-3}$
2	$7.84 \cdot 10^{-3}$	$1.21 \cdot 10^{-2}$	$7.39 \cdot 10^{-3}$	$1.21 \cdot 10^{-2}$	$7.65 \cdot 10^{-3}$	$1.01 \cdot 10^{-2}$
3	$9.34 \cdot 10^{-3}$	$1.22 \cdot 10^{-2}$	$9.33 \cdot 10^{-3}$	$1.22 \cdot 10^{-2}$	$9.49 \cdot 10^{-3}$	$1.02 \cdot 10^{-2}$
4	$1.03 \cdot 10^{-2}$	$1.23 \cdot 10^{-2}$	$1.04 \cdot 10^{-2}$	$1.23 \cdot 10^{-2}$	$1.04 \cdot 10^{-2}$	$1.03 \cdot 10^{-2}$
order	-0.14	-0.01	-0.16	-0.01	-0.13	-0.01

TABLE 12. $\|p - p_{kh}\|$ for the $\mathcal{Q}_2/\mathcal{Q}_1$ discretization with different temporal discretizations and V-projection

level	dG(0)		dG(1)		fractional-step-θ	
	$t = 3 + k$	$t = 6 + k$	$t = 3 + k$	$t = 6 + k$	$t = 3 + k$	$t = 6 + k$
1	$5.78 \cdot 10^{-3}$	$8.83 \cdot 10^{-3}$	$4.34 \cdot 10^{-3}$	$8.81 \cdot 10^{-3}$	$4.74 \cdot 10^{-3}$	$8.82 \cdot 10^{-3}$
2	$7.61 \cdot 10^{-3}$	$8.87 \cdot 10^{-3}$	$7.11 \cdot 10^{-3}$	$8.86 \cdot 10^{-3}$	$7.53 \cdot 10^{-3}$	$8.87 \cdot 10^{-3}$
3	$9.10 \cdot 10^{-3}$	$8.92 \cdot 10^{-3}$	$9.11 \cdot 10^{-3}$	$8.91 \cdot 10^{-3}$	$9.37 \cdot 10^{-3}$	$8.92 \cdot 10^{-3}$
4	$1.00 \cdot 10^{-2}$	$8.95 \cdot 10^{-3}$	$1.01 \cdot 10^{-2}$	$8.95 \cdot 10^{-3}$	$1.02 \cdot 10^{-2}$	$8.95 \cdot 10^{-3}$
order	-0.14	0.00	-0.15	-0.01	-0.12	0.00

TABLE 13. $\|p - p_{kh}\|$ for the cG(1) discretization with different temporal discretizations and repeating one time step

level	dG(0)		dG(1)		fractional-step-θ	
	$t = 3 + k$	$t = 6 + k$	$t = 3 + k$	$t = 6 + k$	$t = 3 + k$	$t = 6 + k$
1	$8.57 \cdot 10^{-2}$	$7.47 \cdot 10^{-1}$	$4.66 \cdot 10^{-2}$	$7.48 \cdot 10^{-1}$	$4.64 \cdot 10^{-2}$	$1.47 \cdot 10^{-1}$
2	$1.52 \cdot 10^{-1}$	$7.50 \cdot 10^{-1}$	$1.01 \cdot 10^{-1}$	$7.51 \cdot 10^{-1}$	$9.90 \cdot 10^{-2}$	$1.48 \cdot 10^{-1}$
3	$2.45 \cdot 10^{-1}$	$7.52 \cdot 10^{-1}$	$2.11 \cdot 10^{-1}$	$7.52 \cdot 10^{-1}$	$1.71 \cdot 10^{-1}$	$1.49 \cdot 10^{-1}$
4	$3.36 \cdot 10^{-1}$	$7.52 \cdot 10^{-1}$	$3.21 \cdot 10^{-1}$	$7.52 \cdot 10^{-1}$	$2.31 \cdot 10^{-1}$	$1.49 \cdot 10^{-1}$
order	-0.46	0.00	-0.61	0.00	-0.43	0.00

5.1.3. Repeating one time step. In this subsection, we present the development of the pressure error when repeating the last time step of the old spatial mesh on the new one to determine the initial values for the first real time step on the new mesh.

The results under uniform temporal refinement are listed in Tables 13–15 for the cG(1), cG(2), and $\mathcal{Q}_2/\mathcal{Q}_1$ spatial discretization, respectively.

We observe for all spatial discretizations that repeating one time step leads to a slower increase of the error in the pressure when switching the spatial mesh from $\mathcal{T}_{2h}$ to $\mathcal{T}_h$ and to an almost constant error when switching from $\mathcal{T}_h$ to $\mathcal{T}_{2h}$.

TABLE 14. $\|p - p_{kh}\|$ for the cG(2) discretization with different temporal discretizations and repeating one time step

level	dG(0)		dG(1)		fractional-step-θ	
	$t = 3 + k$	$t = 6 + k$	$t = 3 + k$	$t = 6 + k$	$t = 3 + k$	$t = 6 + k$
1	$4.14 \cdot 10^{-3}$	$4.41 \cdot 10^{-1}$	$3.26 \cdot 10^{-3}$	$4.46 \cdot 10^{-1}$	$2.95 \cdot 10^{-3}$	$1.01 \cdot 10^{-2}$
2	$6.06 \cdot 10^{-3}$	$4.36 \cdot 10^{-1}$	$5.09 \cdot 10^{-3}$	$4.39 \cdot 10^{-1}$	$5.14 \cdot 10^{-3}$	$1.05 \cdot 10^{-2}$
3	$8.40 \cdot 10^{-3}$	$4.31 \cdot 10^{-1}$	$7.96 \cdot 10^{-3}$	$4.33 \cdot 10^{-1}$	$8.11 \cdot 10^{-3}$	$1.14 \cdot 10^{-2}$
4	$1.04 \cdot 10^{-2}$	$4.27 \cdot 10^{-1}$	$1.03 \cdot 10^{-2}$	$4.28 \cdot 10^{-1}$	$1.03 \cdot 10^{-2}$	$1.22 \cdot 10^{-2}$
order	-0.31	0.01	-0.37	0.02	-0.34	-0.10

TABLE 15. $\|p - p_{kh}\|$ for the $\mathcal{Q}_2/\mathcal{Q}_1$ discretization with different temporal discretizations and repeating one time step

level	dG(0)		dG(1)		fractional-step-θ	
	$t = 3 + k$	$t = 6 + k$	$t = 3 + k$	$t = 6 + k$	$t = 3 + k$	$t = 6 + k$
1	$3.61 \cdot 10^{-3}$	$9.33 \cdot 10^{-3}$	$2.53 \cdot 10^{-3}$	$9.01 \cdot 10^{-3}$	$4.10 \cdot 10^{-3}$	$9.60 \cdot 10^{-3}$
2	$5.74 \cdot 10^{-3}$	$1.00 \cdot 10^{-2}$	$4.70 \cdot 10^{-3}$	$9.66 \cdot 10^{-3}$	$7.12 \cdot 10^{-3}$	$1.07 \cdot 10^{-2}$
3	$8.16 \cdot 10^{-3}$	$1.10 \cdot 10^{-2}$	$7.72 \cdot 10^{-3}$	$1.08 \cdot 10^{-2}$	$9.66 \cdot 10^{-3}$	$1.18 \cdot 10^{-2}$
4	$1.01 \cdot 10^{-2}$	$1.20 \cdot 10^{-2}$	$1.00 \cdot 10^{-2}$	$1.19 \cdot 10^{-2}$	$1.11 \cdot 10^{-2}$	$1.26 \cdot 10^{-2}$
order	-0.31	-0.13	-0.37	-0.14	-0.20	-0.09

Remark 5.1. We remark that the behavior of the fractional-step-θ scheme is hardly a surprise given the results from Section 4.1.2. However, after our analysis in Section 4.2 we can now explain, why the fractional-step-θ scheme doesn't show the undesired divergence of the pressure even without modifications. Namely we saw that the divergence of the pressure is localized to the first time step after changing the mesh. However, in the fractional-step-θ scheme this is only the first substep of a complete time step. Hence, one ignores this "solution" as it is only an intermediate quantity.

5.2. Application to the benchmark problem

We have seen that all three "ideas" are able to (almost) remove the $O(k^{-1})$ increase in the pressure error while the H-projection performed best.

In this subsection, in order to compare all strategies, we return to the benchmark configuration "Laminar Flow Around a Cylinder" with constant inflow and Reynolds number Re = 20 which possesses a stationary solution. The discretization used here is again the cG(1)dG(0) method involving local projection stabilization. In Figure 6, the temporal evolution of the lift-coefficient is depicted for different choices of the initial value. For completeness, we also show the results of the fractional-step-θ scheme combined with a cG(1) discretization in space and local projection stabilization. The upper picture shows the development when switching the spatial mesh from $\mathcal{T}_{2h}$ to $\mathcal{T}_h$ which corresponds to a uniform refinement, while the lower picture

shows the lift-coefficient when switching from $\mathcal{T}_h$ to $\mathcal{T}_{2h}$ which corresponds to a uniform coarsening. The labeling of the different curves is as follows:

- "original": No additional operations are performed when switching the spatial mesh.
- "H-projection": When switching the spatial mesh, the H-projection of the old velocity into the new finite element space is used as initial values for the new time step.
- "V-projection": When switching the spatial mesh, the V-projection of the old velocity into the new finite element space is used as initial values for the new time step.
- "repeat": When switching the spatial mesh, the last time step is repeated already on the new mesh to obtain initial values.

When looking at the upper picture of Figure 6, we note the large error in the lift-coefficient for the "original" method. The curves of the "H-projection" and "V-projection" show a slightly different temporal evolution where the "H-projection" approaches the "original" curve faster. Repeating one time step leads to a temporal evolution of the lift-coefficient which is close to the values produced by the fractional-step-θ scheme.

If we consider the lower picture of Figure 6 which shows the temporal evolution of the lift-coefficient under a uniform coarsening of the spatial mesh, we observe quite large differences between the different strategies. While the "H-projection" mainly eliminates the large error of the "original" curve and stays very close to it elsewhere, the other "ideas" lead to completely different temporal evolutions of the lift-coefficient. Of course, for $t \to \infty$, those values converge to the same stationary limit as the other methods. The fractional-step-θ scheme mainly leads to the same evolution of the lift-coefficient as the "H-projection".

To terminate this subsection, let us reconsider the initial time-dependent benchmark problem. Figure 7 show the temporal evolution of the lift-coefficient after five iterations of adaptive temporal and spatial refinement using dynamic meshes in combination with the H-projection each time the spatial mesh is changed. We observe that the oscillations showing up without using the H-projection when changing the spatial mesh (see Figure 1) have vanished. Furthermore, we note a slightly different temporal evolution of the lift-coefficient, especially at the end of the time interval. This is due to the fact that the adaptive refinement leads to different meshes and time step sizes when applying the H-projection. However, the temporal evolution depicted in Figure 7 is closer to that of the exact solution, see [23].

Conclusions

In this article we analyzed the behavior of the pressure on changing spatial meshes during the computation of nonstationary incompressible fluid flows for several time stepping schemes. In particular we showed that the discrete pressure will in general diverge with order k^{-1} whenever the spatial mesh

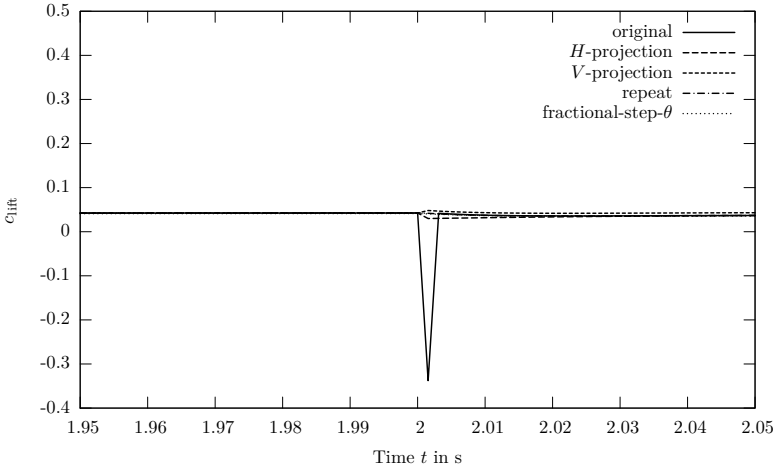

(a) Switching from $\mathcal{T}_{2h}$ to $\mathcal{T}_h$

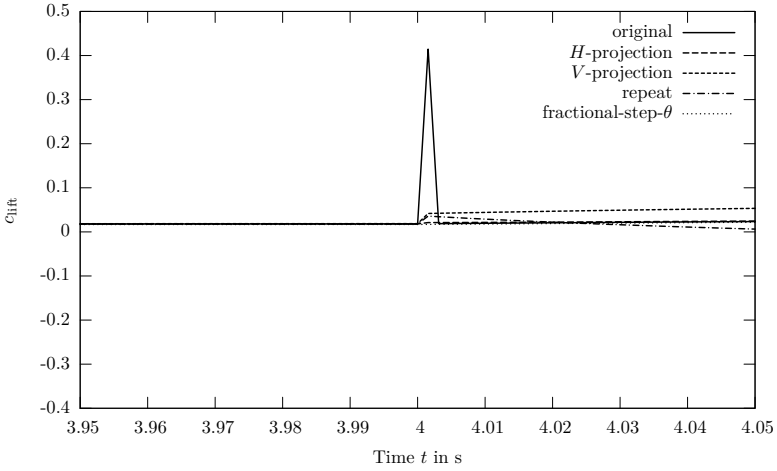

(b) Switching from $\mathcal{T}_h$ to $\mathcal{T}_{2h}$

FIGURE 6. Temporal evolution of the lift-coefficient for different initial values

is changed between two time steps. This behavior is proven, for the dG(0) time-discretization, to be due to the fact that discrete solenoidal vector fields lose this property under changes of the discrete spaces. Finally some possible ways to circumvent the divergence of the pressure are proposed and tested numerically.

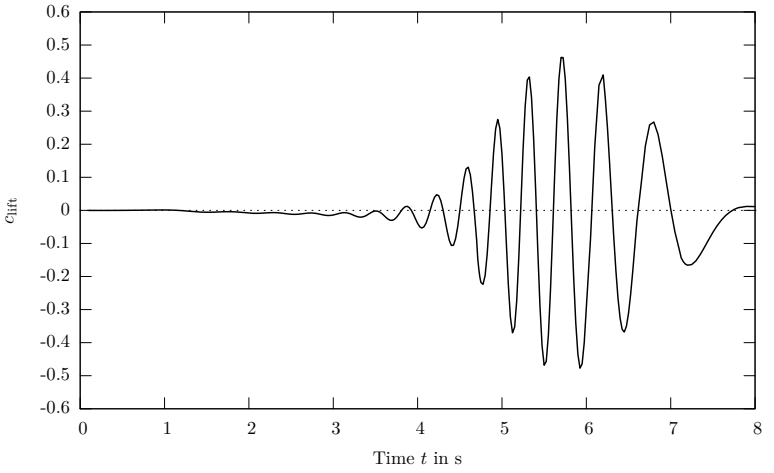

FIGURE 7. Lift-coefficient c_{lift} after five adaptation cycles with H-projection

References

[1] J. P. Aubin. Behavior of the error of the approximate solutions of boundary value problems for linear elliptic operators by Galerkin's and finite difference methods. *Ann. Scuola Norm. Sup. Pisa Cl. Sci. (3)*, 21(4):599–637, 1967.

[2] E. Bänsch. An adaptive finite-element strategy for the three-dimensional time-dependent Navier-Stokes equations. *J. Comput. Appl. Math.*, 36(1):3–28, 1991.

[3] R. Becker and M. Braack. A modification of the least-squares stabilization for the Stokes equations. *Calcolo*, 38(4):173–199, 2001.

[4] R. Becker and M. Braack. A two-level stabilization scheme for the Navier-Stokes equations. In M. Feistauer, V. Dolejší, P. Knobloch, and K. Najzar, editors, *Numerical Mathematics and Advanced Applications. ENUMATH 2003*, pages 123–130, Heidelberg, 2004. Springer-Verlag.

[5] M. Besier. Goal-oriented adaptivity in space-time finite element simulations of nonstationary incompressible flows. Preprint, Universität Heidelberg, 2010.

[6] D. Braess. *Finite Elemente. Theorie, schnelle Löser und Anwendungen in der Elastizitätstheorie*. Springer-Verlag, Berlin Heidelberg New York, second edition, 1997.

[7] F. Brezzi and M. Fortin. *Mixed and Hybrid Finite Element Methods*, volume 15 of *Springer Series in Computational Mathematics*. Springer-Verlag, New York Berlin Heidelberg, 1991.

[8] M. O. Bristeau, R. Glowinski, and J. Periaux. Numerical methods for the Navier-Stokes equations. applications to the simulation of compressible and incompressible viscous flows. *Computer Physics Reports*, 6(1–6):73–187, 1987.

[9] G. F. Carey and J. T. Oden. *Finite Elements. Volume III. Computational Aspects*. The Texas Finite Element Series. Prentice-Hall, Inc., Englewood Cliffs, 1984.

[10] P. G. Ciarlet. *The Finite Element Method for Elliptic Problems*. North-Holland Publishing Company, Amsterdam New York Oxford, first edition, 1987.

[11] P. Clément. Approximation by finite element functions using local regularization. *RAIRO Anal. Numér.*, 9(R-2):77–84, 1975.

[12] M. Dauge. Stationary Stokes and Navier-Stokes systems on two- or three-dimensional domains with corners. Part I: Linearized equations. *SIAM J. Math. Anal.*, 20(1):74–97, 1989.

[13] deal.II, A Finite Element Differential Equations Analysis Library. `http://www.dealii.org/`.

[14] K. Eriksson, D. Estep, P. Hansbo, and C. Johnson. Introduction to adaptive methods for differential equations. In A. Iserles, editor, *Acta Numerica 1995*, volume 4, pages 105–158. Cambridge University Press, Cambridge, 1995.

[15] K. Eriksson, D. Estep, P. Hansbo, and C. Johnson. *Computational Differential Equations*. Cambridge University Press, 1996.

[16] Gascoigne, High Performance Adaptive Finite Element Toolkit. `http://www.gascoigne.uni-hd.de/`.

[17] V. Girault and P.-A. Raviart. *Finite Element Methods for Navier-Stokes Equations. Theory and Algorithms*, volume 5 of *Springer Series in Computational Mathematics*. Springer-Verlag, Berlin Heidelberg New York Tokyo, 1986.

[18] R. Glowinski. Finite element methods for incompressible viscous flow. In P. G. Ciarlet and J. L. Lions, editors, *Numerical Methods for Fluids (Part 3)*, volume 9 of *Handbook of Numerical Analysis*, pages 3–1776. North Holland, Amsterdam, 2003.

[19] J. G. Heywood and R. Rannacher. Finite element approximation of the nonstationary Navier-Stokes problem. I: Regularity of solutions and second-order error estimates for spatial discretization. *SIAM J. Numer. Anal.*, 19(2):275–311, 1982.

[20] J. G. Heywood, R. Rannacher, and S. Turek. Artificial boundaries and flux and pressure conditions for the incompressible Navier-Stokes equations. *Internat. J. Numer. Methods Fluids*, 22(5):325–352, 1996.

[21] J. Hoffman and C. Johnson. Adaptive finite element methods for incompressible fluid flow. In T. J. Barth and H. Deconinck, editors, *Error Estimation and Adaptive Discretization Methods in Computational Fluid Dynamics*, volume 25 of *Lecture Notes in Computational Science and Engineering*, pages 97–158. Springer-Verlag, Heidelberg, 2003.

[22] P. Hood and C. Taylor. Navier-Stokes equations using mixed interpolation. In J. T. Oden, O. C. Zienkiewicz, R. H. Gallagher, and C. Taylor, editors, *Finite Element Methods in Flow Problems*, pages 121–132, Huntsville, 1974. University of Alabama.

[23] V. John. Reference values for drag and lift of a two-dimensional time-dependent flow around a cylinder. *Internat. J. Numer. Methods Fluids*, 44(7):777–788, 2004.

[24] R. B. Kellogg and J. E. Osborn. A regularity result for the Stokes problem in a convex polygon. *J. Funct. Anal.*, 21(4):397–431, 1976.

[25] P. Klouček and F. S. Rys. Stability of the fractional step θ-scheme for the nonstationary Navier-Stokes equations. *SIAM J. Numer. Anal.*, 31(5):1312–1335, 1994.

[26] G. Nabh. *On High Order Methods for the Stationary Incompressible Navier-Stokes Equations*. PhD thesis, Universität Heidelberg, Heidelberg, 1998.

[27] J. Nitsche. Ein Kriterium für die Quasi-Optimalität des Ritzschen Verfahrens. *Numer. Math.*, 11:346–348, 1968.

[28] M. Schäfer and S. Turek. Benchmark computations of laminar flow around a cylinder. In E. H. Hirschel, editor, *Flow Simulation with High-Performance Computer II*, volume 52 of *Notes on Numerical Fluid Mechanics*, pages 547–566, Braunschweig Wiesbaden, 1996. Vieweg.

[29] M. Schmich. *Adaptive Finite Element Methods for Computing Nonstationary Incompressible Flows*. PhD thesis, Universität Heidelberg, Heidelberg, 2009.

[30] R. Temam. *Navier-Stokes Equations: Theory and Numerical Analysis*. AMS Chelsea Publishing, Providence, Rhode Island, 2001.

[31] V. Thomée. *Galerkin Finite Element Methods for Parabolic Problems*, volume 25 of *Springer Series in Computational Mathematics*. Springer-Verlag, Berlin Heidelberg, 1997.

[32] S. Turek. A comparative study of time-stepping techniques for the incompressible Navier-Stokes equations: From fully implicit non-linear schemes to semi-implicit projection methods. *Internat. J. Numer. Methods Fluids*, 22(10):987–1011, 1996.

[33] S. Turek. *Efficient Solvers for Incompressible Flow Problems. An Algorithmic and Computational Approach*, volume 6 of *Lecture Notes in Computational Science and Engineering*. Springer-Verlag, Berlin Heidelberg, 1999.

[34] R. Verfürth. *A Review of A Posteriori Error Estimation and Adaptive Mesh-Refinement Techniques*. Wiley-Teubner Series Advances in Numerical Mathematics. Wiley-Teubner, New York Stuttgart, 1996.

Michael Besier
Im Neuenheimer Feld 293/294
69120 Heidelberg
Germany
e-mail: michael.besier@iwr.uni-heidelberg.de

Winnifried Wollner
Im Neuenheimer Feld 293/294
69120 Heidelberg
Germany
e-mail: winnfried.wollner@iwr.uni-heidelberg.de